University of Alberta

STUDY OF THE RESPONSE OF PICASSO BUBBLE DETECTORS TO NEUTRON IRRADIATION

by

Daniiar Marlisov

A thesis submitted to the Faculty of Graduate Studies and Research
in partial fulfillment of the requirements for the degree of

Master of Science

Department of Physics

Spring 2013
Edmonton, Alberta

I dedicate my thesis to my mother, to my grandmother and to Kyrgyzstan.

To Have and to Lose, Chingiz Aitmatov.

Oh, Issyk-Kul, my Issyk-Kul–my unfinished song!
Why did I have to remember that day when I came here with YOU and stopped on the same rise, right above the water?
Everything was the same. The blue-and-white waves ran up the yellow shore holding hands.
The sun was setting behind the mountains, and at the far end of the lake the water was tinged with pink.
The swans wheeled over the water with excited, exultant cries.
They soared up and dropped down on outspread wings that seemed to hum.
They whipped up the water and started wide, foaming circles.
Everything was the same, only there wasn't YOU with me.
Where are you, my slender poplar in a red kerchief, where are you now?

Abstract

The objective of this work was to simulate the PICASSO experiment and to study the detector response to neutron irradiation. The results of the simulation show the rock neutron rate to be 1-2 neutrons/day for the setup used until 2009 and less than 0.1 neutrons/day for the setup used after 2010. The shielding efficiency was calculated to be 98% and 99.6% for the two setups respectively. The detector response to an AmBe source was simulated. Neutron rates differ for two AmBe source spectra from the literature. The observed data rate is in agreement with the rate from the simulation. The detector stability was examined and found to be stable. The source position and orientation affect the detector efficiency creating a systematic uncertainity on the order of 10-35%. This uncertainity was eliminated with a source holder. The localisation of recorded events inside the detector and the simulated neutron distribution agree.

Acknowledgements

The first thanks will go to my supervisor Carsten Krauss. Thanks for him for e-mailing me and showing interest when I just arrived to Edmonton. I liked him for his personality, because he can always find time to help even if he is very busy. He taught me everything that I know right now. Thank you Carsten for this thesis. He is the first and the best supervisor of mine.

I would also like to thank PICASSO members for letting me to live in their ”cute family”, a special thanks to Rob. Thank you very much Solange for your endless help, you used to always listen to me and help me with all my problems.

I would like to thank the department of physics of university of Alberta for providing such a nice environment. And I thank the members of astro-particle group, especially Logan for his help when I just started programming.

Thanks to Kingsley, Pitam, Kari, Nooshin for being my friends and for their help, it was really fun to study in here with you guys. I like how we are good friends even if have different beliefs and different background. Thank you guys for lunch times, soccer games and everything else. Thanks to xtachx and NooshX for ”research” times too.

Very special thanks to Naku. She was the one who was not interested in what I do in the university but used to support and help me with everything. Thanks for being in my world. I like when you describe what dark matter is.

I would like to thank my mom, my tainem (grandma), my sister Emu, brothers Talgar and Beka for being the reason for me to study here.

Table of Contents

List of Tables

List of Figures

Chapter 1

Introduction

Science is the study of the structure and behavior of the nature through observations and experiments. The structure and behavior of the world surrounding us are difficult to understand, where most is a mystery and unknown. The universe exists in an extraordinary and a wonderful way, everything in it from tiny particles to huge galaxies is amazing to study. One of the marvelous subjects which is a challenge to explore and understand is the topic of Dark Matter. By looking outside the Earth, only dark and free space sparsely filled with stars, planets and dust can be seen. About 80 years ago astronomer Fritz Zwicky investigated the motion of galaxy clusters and established evidence for unseen dark matter by observing more mass in a galaxy cluster from its speed than what was expected from its luminosity. Nowadays, more evidence proves that there is dark matter which is not visible and which does not interact with baryonic matter. This unseen or dark matter makes our universe behave as it does today. It was found that 85% of the matter in the universe cannot be seen or be detected. This invisible matter is generally expected to be in non-baryonic form. Many experiments are running today to detect a particle called WIMP (Weakly Interacting Massive Particle) an elementary particle of a dark matter. One such experiment is the Project In Canada to Search for Supersymmetric Objects (PICASSO).

PICASSO is a threshold bubble detector experiment built to detect the WIMP directly using superheated droplet detectors that are installed 2km underground at SNOLAB in Sudbury, Ontario. It uses cylindrically shaped acrylic containers filled with liquid that contain tiny superheated C_4F_{10} droplets. When a WIMP interacts with an atom within a C_4F_{10} droplet and deposits enough energy, the droplet undergoes a phase transition and becomes a gas bubble creating noise which is received by piezo-electric sensors which are attached on the walls of the acrylic containers. The whole experiment is shielded with water to protect the detectors from neutrons coming from the surrounding rock in the lab. The detectors are not sensitive to gammas in the temperature range of interest.

The main objective of this thesis was to study the detector response to neutrons. Neutrons create nuclear recoils in the detectors and WIMPs are also expected to create nuclear recoils, that is why neutrons are used to study the detector properties. In this thesis, a simulation of the PICASSO experiment, simulating the detector response to neutrons using the Geant4 simulation toolkit is presented. The results from the simulation are compared with the experimental neutron calibration data. The neutron background from the rock and the efficiency of the water shield was studied using a simulation of neutron propagation in the detector. The neutron flux and energy spectrum from the rock has been simulated. The results are compared to recent studies, which verifies the simulation. The detector response to an AmBe neutron source was studied to determine the efficiencies of the detectors, and to study the propagation of neutrons inside PICASSO, and to verify the positioning of the source. Studies include the stability of detectors as a function of time. Moreover, the study of neutron rates as a function of temperature is shown. The theory and simulation of multiple interactions of a single neutron in PICASSO is described.

In chapter 2, the dark matter problem is discussed, with information about the evidence for invisible mass, dark matter properties and dark matter search experiments. A detailed description of the PICASSO experiment and its detectors is given in chapter 3, with full information of the operation of the experiment. In chapter 4 a study of the detector response to neutrons from the rock and the efficiency of the water shielding are presented. Finally, chapter 5 contains studies of the bubble detector response to AmBe source neutrons. Efficiencies of detectors are simulated which are compared to the data. A summary of the results and conclusion of the thesis is given at the end.

Chapter 2

Dark Matter

2.A Unsolved Mystery

Every human being would like to know the history of the universe, the present state of the world and a little about the future. Each person can relate the above statement to their own background. Scientists see in it the Big Bang, the expansion, the development and the future progress of the universe. The observation of the WIMP (Weakly Interacting Massive Particle), a dark matter particle candidate, will help scientists test the validity of current theories of the origin and evolution of the universe. Finding its properties will help to understand how the universe formed, and how it will end.

In the 20^{th} Century astronomers using telescopes started to estimate the speed and the mass of distant stars and galaxies. Before, scientists thought they knew that the universe was a finite space with galaxies in it. However, they found out, that no matter which direction they pointed their telescopes the observed light is red shifted [15]. Observing red-shifted galaxies in every direction implies expansion in all directions. After the Big Bang, the generated matter expanded evenly in all directions. Matter then started to clump together, attracted by gravity, to form stars and galaxies as observed today. But there is dark energy (unexplained energy that makes the universe expand) with a strong field that overcomes gravity and forces galaxies to move apart from each other faster and faster. One of the problems of the Big Bang theory is to explain how the planets, galaxies and stars were formed if the dark energy expands the space between matter, which results as a repulsive force between matter. Scientists postulate that dark matter provides the attractive force that clumps matter together. The second question astronomers ask is how this expansion is going to end. Is it going to stop or is it going to continue, or is the universe going to be pulled inward by gravity at some point? It is currently believed that the universe will continue to expand forever. The density and distribution of dark matter has been measured but the nature of dark matter as particles is still unknown.

2.B Observational Evidence for Dark Matter

In earlier years, people used to treat the universe as stars, planets and gas. Observations then found that there is more matter than just the visible matter. This extra matter is dark matter. This invisible component of the universe can be detected indirectly, by its gravitational effects on luminous matter. There are many lines of evidences from different groups of scientists, who use different instruments and who approach dark matter with different perspectives, but all of them report the same amount of invisible matter. There are several experiments detecting the gravitational effects of dark matter by measuring the mass of galaxies, which are:

- Measuring the velocities of galaxy clusters and galaxies using Dopplers shift and calculating the overall mass.
- Measuring the mass of galaxy clusters using gravitational lensing.

Examples for all the above counted problems and experiments are given in the following paragraphs.

2.B.1 Rotation and motion of clusters and galaxies

Fritz Zwicky's observation

In 1933, swiss Astronomer, Fritz Zwicky, while working at the California Institute of Technology (Caltech), noticed while studying the Coma galaxy cluster some unexplained features in the luminosity of galaxies in the cluster. He calculated the expected rotational speed of galaxies in that cluster using the masses derived from the luminosity of stars. The speed of galaxies he observed is 160 times larger than what could be expected from Newton's 2^{nd} law [14]. To account for this meant that there was a missing or unseen mass 159 times the mass of the visible matter. It was later determined that Zwicky was the discoverer of dark matter.

Vera Rubin on Rotational Curves of Spiral Galaxies

In 1973 Vera Rubin and her colleague Kent Ford examined the velocities of stars in spiral galaxies. They demonstrated that the velocities of stars appear not obey Newton's laws of gravity. They found that all stars far away from the galactic centre move with almost the same speed as the closest stars (Figure 2.1), they were not able to understand the force that holds those stars in

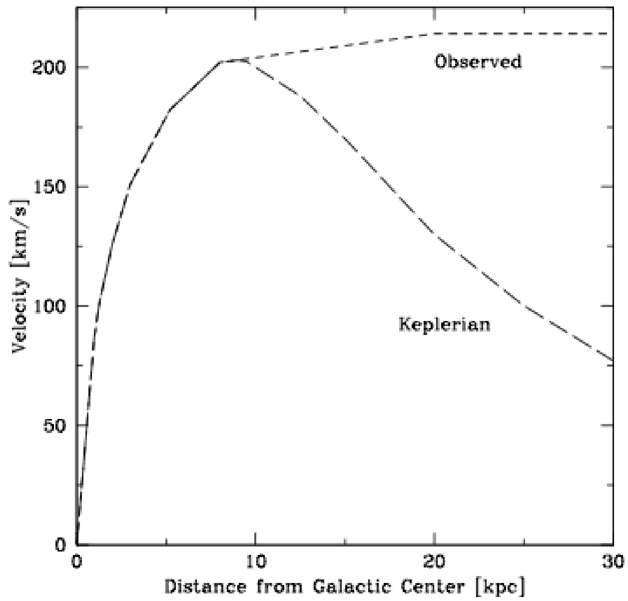

Figure 2.1: The expected velocities of the stars inside the spiral galaxy and the observed velocities from the centre of the spiral galaxy [42].

their orbits [14]. So, their first solution to this dramatic observation was: there should be a mass that does not interact via electromagnetic force which therefore is not visible that is 10 times heavier than visible matter and the only force it interacts with is the gravitational force.

Galaxies moving toward each other

The most current simulations about the number of galaxies in the universe predict about 500 billion galaxies in the universe. And most galaxies and groups of galaxies approach each other by a gravitational pull with larger velocities than expected. For instance, the Milky Way is moving rapidly towards Andromeda with a speed 3×10^5 km/h. This proves the existence of dark matter [34], because if these two galaxies had only the amount of mass that is visible they would not be able to achieve the speed they move with. In order to move with the above velocity they need at least 10 times more mass than is visible.

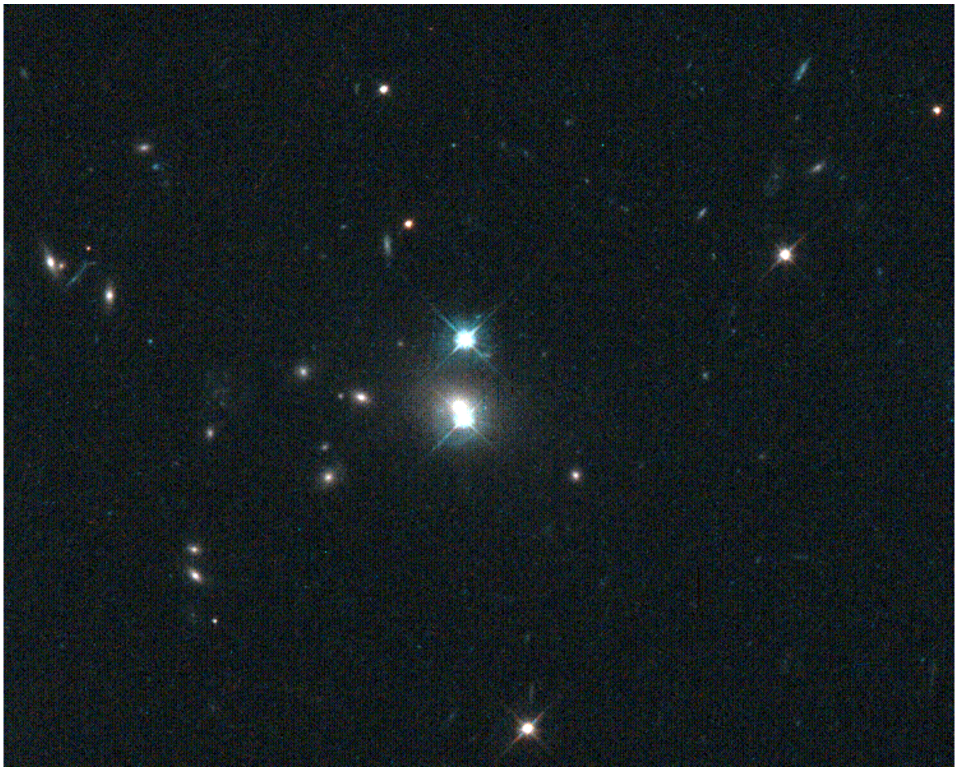

Figure 2.2: The image of identical quasars taken in 1979 [40].

2.B.2 Gravitational lensing

More evidence for dark matter comes from gravitational lensing experiments. According to Einstein's general theory of relativity the gravitational field bends the path of light rays. This can be used to prove the existence of more mass than the visible mass in galaxy clusters. If the theory of dark matter is true, then the light that travels next to any cluster will be bent more, because the mass of a cluster is larger than the luminous mass of components of that cluster. In 1979 scientists observed identical twin quasars. They were so similar that observers thought that they were just images of one very distant object (shown in Figure 2.2), a quasar [22]. Detailed searches showed a faint elliptical galaxy next to the twin quasars, where it was determined that this image is an astronomical object between Earth and a very distant quasar, which proved gravitational lensing. More and more evidence is found using gravitational lensing proving the existence of hidden mass in the universe.

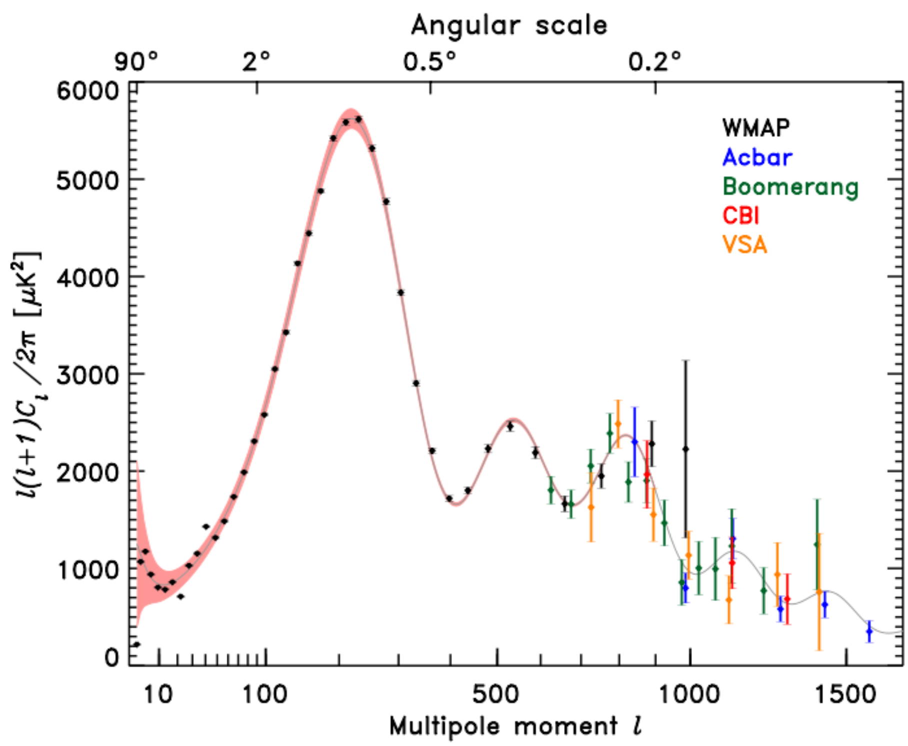

Figure 2.3: Data has been taken from WMAP, Acbar, Boomerang, CBI and VSA instruments that have been fitted by theoretical model. It represents the power spectrum of the cosmic microwave background radiation temperature anisotropy in terms of the angular scale and multipole moment [35].

2.B.3 CMBR

Cosmic microwave background radiation (CMBR) is thermal radiation filling the universe. After the Big Bang the universe was so hot that there were lots of photons produced by black body radiation from dense, hot plasma. Some thermal radiation which was emitted at that time is reaching the Earth now. Using sufficiently sensitive instruments a faint signal from very dark space can be measured. This signal is consistent in all directions which demonstrates that it is not associated with any star, galaxy, or other object and it is well explained as radiation left over from an early stage in the development of the universe. The microwave region tells us that the galaxies are moving apart from each other, isotropic and homogeneous background radiation tells us it is expanding in all directions [33]. However, the background radiation is not perfectly isotropic and homogeneous. There are some fluctuations in the radiation power spectrum. Scientists plotted a graph of the cosmic microwave background radiation power spectrum in terms of angular scale which is shown in Figure 2.3. The main peak tells us about the curvature shape of the universe, where the second peak shows the density of baryonic matter in space and from the third peak information about the density of the dark matter can be deduced [35]. Although many different processes might produce the CMBR, no model other than the Big Bang has yet explained the fluctuations. As a result, most cosmologists consider the Big Bang model of the universe to be the best explanation for the CMBR. It explains the existence and structure of the cosmic microwave background, the large scale structure of galaxy clusters, the distribution of baryonic matter and the accelerating expansion of the universe, and provides a measurement of the dark matter density of the universe.

2.C Definition of dark matter

Dark matter is by definition dark, which means it is not in the form of normal easily observable matter, or in other words it does not interact via electromagnetic force. To date it has only been detected by its gravitational effect and it is also expected to interact by the weak force. Dark matter explains how galaxies, clusters and super clusters of galaxies formed and behave in the universe. Scientists classify dark matter into three groups: hot, warm and cold dark matter according to its energy. The first category, hot dark matter, is a hypothetical form of dark matter which consists of particles that travel with relativistic velocities. The best candidate for the identity of hot dark matter is the neutrino [21]. Neutrinos have very small masses, and do not interact with light, do not interact through the strong force, they do interact by the weak force, and gravity, but due to the weak strength of these interactions they are difficult to observe. Hot dark matter can explain the formation of structures like superclusters, but when it comes to small scale structures like galaxies it fails to explain the formation of galaxies from the Big Bang. It is nearly impossible for very light and fast moving particles to clump together and form small scale galaxies and planets. To explain the small scale structure in the universe it is necessary to have cold or warm dark matter. Warm dark matter is a second form of dark matter that has properties between those of hot dark matter and cold dark matter. The most common candidates for this type of dark matter are sterile neutrinos and gravitinos [10]. It seems that hot and warm dark matter can make up a small fraction of the dark matter in the universe, but most of the dark matter is probably of some other form, which is considered to be cold dark matter. Cold dark matter is made of particles that move at classical (non-relativistic) velocities and it is currently the area of greatest interest for dark matter researchers to explain the formation and structure of the universe. Physicists expect cold dark matter to be the best answer to explain the distribution of galaxies and clusters seen today.

2.D WIMP as dark matter

According to observations dark matter:

- is made up of heavy massive particles from its huge gravitational pull.
- is made up of stable particles that do not decay.
- does not interact via electromagnetic force, which means that it is neutral.
- is non-baryonic matter.
- does not interact through the strong force, otherwise the universe would have collapsed [24].
- is mostly non-relativistic or cold dark matter, if it was relativistic or hot like neutrinos it would not be able to explain the formation of galaxies from the Big Bang theory [25].
- is assumed that dark matter particles interact with the weak force.

There are many dark matter candidates proposed by theory, but among all of them the most favourable candidate is the Weakly Interacting Massive Particle (WIMP). After the Big Bang the universe was so hot that the rate at which new particles were created was equal to the rate at which particles were annihilated. By the time the universe expanded and cooled, no more new particles were thermally produced, but the particle annihilation processes continued. Nowadays, only leftover particles exist in the universe, the annihilation rate is negligibly small. WIMPs are believed to be one of those leftover particles. A WIMP is a hypothetical particle that can explain dark matter observations. It does interact through the weak force and the gravitational force, but neither scatters light, nor reacts to the strong force. It moves slowly, is a non-relativistic particle, and it is 50-100 times heavier than a neutron or a proton. Supersymmetry theory predicts a particle that has the same properties as the WIMP. Therefore WIMP is a favourite particle for dark matter searches. Only a particle that has the properties of a WIMP can explain all observations, because there is insufficient baryonic matter to account for the measured amount of dark matter and galaxy formation models involving WIMPs match observations of the large-scale structure [31]. According to large scale structure simulations the universe is full of WIMPs and galaxies formed around clumps of WIMPs. The theory can explain rapidly moving galaxies and clusters and the bending of light coming from distant galaxies. There is no Standard Model particle that has the same properties as the WIMP. One of the particles that can be a WIMP is the neutralino [16]. Neutralinos are one of the SUSY (supersymmetry) particles. They are a mixture of neutral Higgsino, the superpartner of Higgs Boson, Wino and Bino, which are neutral electroweak gauginos (superpartners of gauge bosons). The MSSM (Minimal Supersymmetric Standard Model) predicts 4 neutralinos that are fermions with spin 1/2 and are electrically neutral. The neutralino is expected to have a mass between 50 GeV and 1 TeV. In R-parity conserving models, the lightest neutralino is stable and all other supersymmetric particles end up decaying into lightest supersymmetric particle (LSP). In addition to neutralinos there are other superparticles that can be WIMP candidates, as superpartners of the tau lepton, the top quark, the neutrino and the graviton [13]. WIMPs tend to interact with an atom's nucleus causing a nuclear recoil in detectors by the weak force which provides a possible means of detecting them.

2.E Search Techniques and Experiments

2.E.1 Detection Methods

WIMPs can be detected through three different complementary methods. They can be produced then detected indirectly, they can be detected indirectly and can be observed directly.

1. The first approach to detect WIMPs is to produce them by colliding proton beams at the LHC (Large Hadron Collider). After proton proton interaction many particles are produced. One of those particles can be a WIMP and since it has negligible interaction with matter, the signature of WIMP production at the LHC would be large amounts of missing energy and momentum in a collision. The missing energy and momentum would indicate a WIMP that escaped the detection, not interacting with any matter or being caught in any sensitive devices [26].

2. Indirect detection of WIMPs means not to detect the WIMPs themselves but to detect particles that are created by WIMP-WIMP annihilation. WIMPs are thought to be Majorana particles, particles that are identical to their anti-particles, which can undergo WIMP-WIMP annihilation. If

this kind of interaction occurs a distinctive signal in the form of high energy neutrinos would be observed. Even if the WIMPs are not Majorana particles, but Dirac particles then it may still possible to see WIMP-WIMP annihilations, if the density of particle and its anti-particle are comparable [29]. WIMPs usually do not interact with each other. If interactions happen they would occur more often in WIMP dense regions, for instance in the core of astronomical objects like the Sun or the Earth. It is generally agreed that the detection of signals of WIMP-WIMP annihilation would be the strongest indirect proof of WIMP dark matter. Research groups like IceCube, ANTARES and SuperKamiokande are collecting data in different parts of the world to evaluate the existence of dark matter with indirect detection.

3. Direct detection means to detect the WIMP signal directly when it interacts with any Standard Model particle. If the WIMP is a particle that was created in the early universe, and if it does annihilate, it would interact with ordinary baryonic particles. A WIMP would be expected to scatter off atomic nuclei elastically and deposit a measurable amount of energy in a detector. Direct detection experiments are designed in such a way that they are very sensitive to a tiny perturbation inside their active volumes. Sensors, attached to the detector surface, record the sound, or heat, or vibration that is created due to the interaction inside the detector medium. There are different types of detectors to search for WIMPs directly like Cryogenic detectors, Noble liquid detectors and superheated liquid detectors, where every detector is designed to detect WIMP with their own technologies [29].

2.E.2 Types of detectors

There are several types of detectors that use the direct detection method, but different detection techniques.

1. Superheated Liquid Detectors. These detectors can be made insensitive to low deposited energy densities by tuning thermodynamic parameters like temperature and pressure. Or in other words, these detectors are sensitive only to nuclear recoils which provide enough energy to cause a nucleation while they are insensitive to gamma rays and other particles that interact with electrons. The backgrounds for these detectors are produced by neutrons and alpha decays from radioactive contamination in the detector. This technique is capable of distinguishing background particles which scatter off electrons, from dark matter particles which scatter off nuclei. Experiments that use superheated liquid detector technology include COUPP, PICASSO and SIMPLE [26].

2. Noble Liquid Detectors detect the flash of scintillation light produced by a particle collision in liquid xenon or argon [29]. They are also capable of distinguishing background particles which scatter off electrons, from dark matter particles which scatter off nuclei. Noble liquid experiments include: ZEPLIN, XENON, DEAP, ArDM, WARP, LUX, Dark Side and XMASS.

3. Cryogenic detectors operate at very low temperatures (below 100mK [26]) to search for dark matter particles. This approach detects the heat and lattice vibrations produced when a particle hits an atom in a crystal absorber such as germanium. Heat and lattice vibrations can be used

to distinguish different types of interactions. Cryogenic detectors with improved designs and strong background discrimination can achieve very low energy thresholds and are used widely all over the world. Cryogenic detector experiments include: CDMS, CRESST and EDELWEISS.

2.E.3 Dark Matter Search Experiments

CDMS

One of the direct WIMP detection dark matter search experiments is CDMS (Cryogenic Dark Matter Search) [37]. The current experiment CDMSII is located underground in the Soudan mine in Minnesota, USA. The CDMS detector is an array of disks of germanium, cooled to extremely low temperatures (mK) that are needed to reduce the thermal noise that would otherwise hide the phonon signal. On the surfaces of the detector crystals hundreds of small thermometers are located. When a WIMP passes through a crystal it interacts with an atom, as a result heat is produced which is detected by the thermometers. Detectors measure the ionization and phonons produced by every particle interaction in the germanium crystals. In every interaction they are able to read out the type and the energy of the particle. The ionization signal is produced by interaction between the radiated electrons from the germanium, where the phonon interaction is produced by nuclear interactions. The vast majority of background particle interactions are electron interactions, while WIMPs (and neutrons) are expected to produce nuclear recoils. Unwanted neutrons from outside of the experiment are removed by polyethylene absorbers. This allows the vast majority of the unwanted background interactions to be rejected, so that any WIMP-scattering events can be identified even if they are very rare. CDMS 2011 results that focused on reanalyzing 2006-2008 data with a lowered threshold and increased sensitivity did not observe any WIMP signal.

XENON

XENON is a Dark Matter direct detection experiment, which uses liquid xenon as detector medium that is located at the Gran Sasso underground laboratory in Italy. The current phase of the experiment is XENON100 with 100 kg of liquid xenon as target material with 50 times better sensitivity compared to the old detector [43]. When a dark matter particle interacts with a xenon nucleus inside the xenon liquid a scintillation light is produced which is then detected by photomultipliers. The ionization electrons are separated from the Xe ions and drifted upwards by a strong electric field. Putting more active liquid into the detector the collaboration aims to build a detector with the best WIMP sensitivity, while at the same time reducing the gamma background by a factor of 100 by a careful selection of all detector materials. In order to shield the target volume even further they surrounded the detector completely by a layer of liquid xenon. XENON plans to probe the lowest SUSY parameter space, with a sensitivity of 1 event/100 kg/year. The XENON100 collaboration recently published new results using 62 kg of liquid xenon in an ultra-low background dual-phase time projection chamber. According to data of 11.17 live days, XENON100 did not observe any events and excluded WIMP-nucleon elastic scattering cross-sections above $3.4 \times 10^{-44} cm^2$ for 55GeV/c^2 WIMPs at the 90% confidence level [3].

DEAP

DEAP (Dark Matter Experiment using Argon Pulse-shape discrimination) is a direct dark matter search experiment that uses argon as a target material. DEAP is constructing a new detector with 3600 kg of active material and it will have sensitivity to WIMP-nucleon scattering cross-sections as low as $10^{-46} cm^2$ for a WIMP mass of $100\text{GeV}/c^2$ [38]. As for all noble liquid detectors gamma rays that pass through the liquid medium are the largest potential background for DEAP. Fortunately, the time structure of the scintillation light signal is different for nuclear recoils, signals from a WIMP, and for electron recoils, caused by argon beta decay and natural radioactivity are discriminated with extremely high efficiency.

COUPP

COUPP (Chicagoland Observatory for Underground Particle Physics) is an experiment at SNOLAB to detect dark matter with 60 kg of heavy liquid at room temperature in a bubble chamber detector. COUPP is based on the same idea of particle detection as PICASSO, they both use the superheated liquid technique. Fluorine and iodine are the target materials in a superheated metastable state dispersed inside a liquid to keep them non-disturbed, when a WIMP interacts with nuclei the liquid forms a protobubble that becomes larger creating noise. The noise is then picked up by piezo-electric sensors and the waveform is stored for analysis. The main difference between COUPP and PICASSO is that COUPP has more active mass [36].

2.F Spin Dependent, Spin Independent Searches

The main efforts in the direct dark matter search experiments are concentrated in the field of elastically spin-independent (scalar) and spin-dependent (axial vector) WIMP-nucleon interaction. In spin-independent (SI) scattering the WIMP couples with a nucleon through Higgs particle exchange and in spin-dependent (SD) scattering it happens through Z particle exchange. In SI interaction the WIMP coupling is proportional to the mass of the nucleus, where in SD interaction the WIMP coupling is proportional to the spin of the nucleus. SD interactions only occur if the target nucleus is an odd isotope.

The WIMP-nucleus cross-section has two different terms (SI and SD terms) [29]. For SI searches the first term is used and for SD interaction the second term of the equation 2.1 is used.

$$\sigma_{0WN} = \frac{4\mu_A^2 v^2}{\pi}[Zf_p + (A-Z)f_n]^2 + \frac{32G_F^2\mu_A^2}{\pi}\frac{J+1}{J}(a_p\langle S_p\rangle + a_n\langle S_n\rangle)^2 \quad (2.1)$$

Where in the equation G_F is the fermi coupling constant, f_p and f_n (a_p and a_n) are effective spin-independent (spin-dependent) couplings of the WIMP to the proton and neutron, respectively. To get the differential cross-section the following equation is used:

$$\frac{d\sigma_{WN}(q)}{dq^2} = \frac{1}{\pi v^2}|M^2| = \frac{\sigma_{0WN}F^2(q)}{4\mu_A^2 v^2} \quad (2.2)$$

Here, v is the velocity of the WIMP, F is a form factor describing the spatial extension of the nucleus, $\mu_A = \frac{M_X M_A}{M_X + M_A}$ is the WIMP-nucleus reduced mass (WIMP mass M_X, target nucleus mass M_A). SI WIMP-nucleus cross-section observations can be used to compare experimental results to theory and to each other. While SD WIMP-nucleus cross-section measurements cannot be easily compared to each other since spin dependence is related to one of two possible nuclei; proton or neutron.

The results currently obtained in the dark matter search experiments are usually presented in the form of exclusion curves. For a fixed mass of the WIMP the values of the cross-section of elastic WIMP-nucleon interaction located above these curves are excluded experimentally. Unfortunately, up to this time none of the dark matter experiments have managed to see any evidence of a WIMP. But there are results for exclusion limits on the WIMP-nucleon cross-section for most experiments. These limits are based on WIMP-nucleon cross-section as a function of a WIMP mass. Figure 2.4 shows SD and SI exclusion graphs for several experiments.

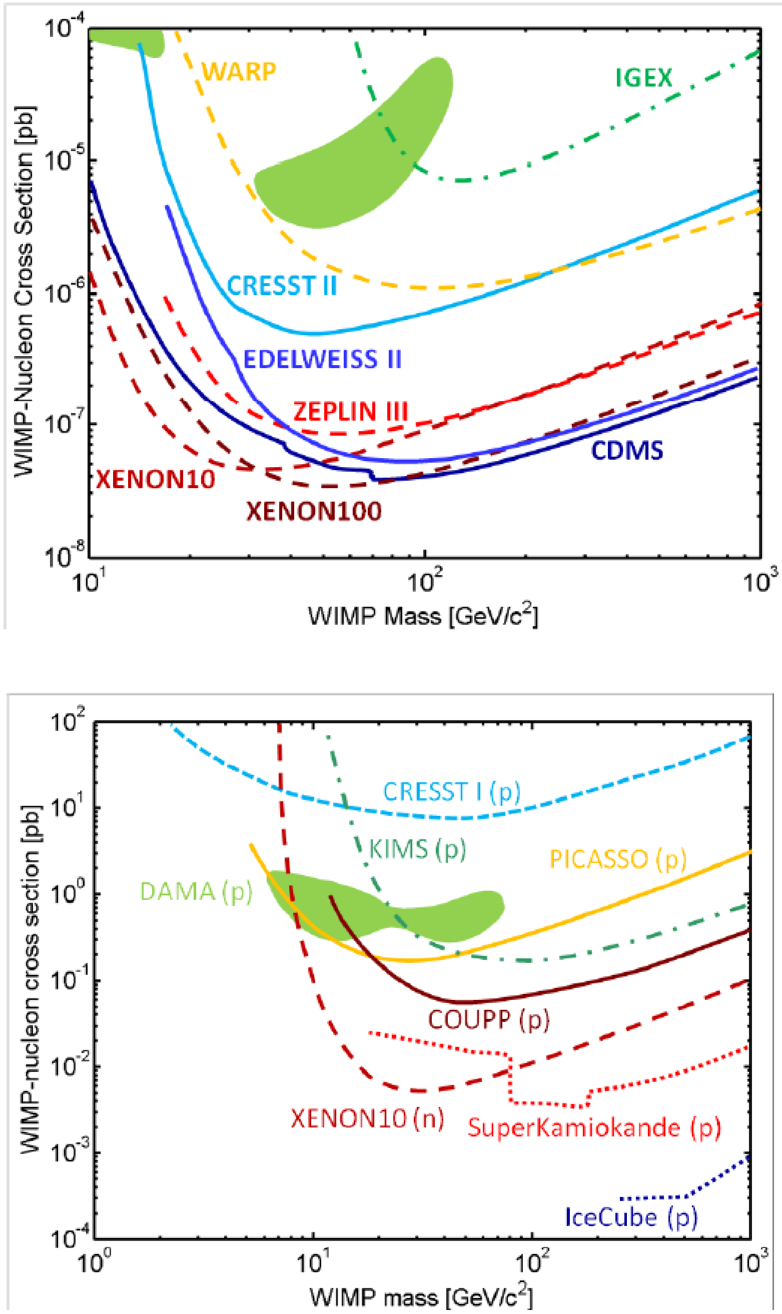

Figure 2.4: These exclusion plots show the limits for spin-independent and spin-dependent WIMP-nucleon interaction for some experiments. [26].

Chapter 3

PICASSO

The Project in Canada to Search for Supersymmetric Objects (PICASSO) is an experiment that is built to detect Dark Matter particles 2 kilometers underground at SNOLAB, Sudbury, Ontario, Canada.

3.A Detection Principle

PICASSO is searching for WIMPs using the superheated liquid technique with fluorine as active material. A superheated liquid is defined as a fluid held at a temperature greater than the boiling point of that liquid. In such a metastable state, it can only remain stable if it is not disturbed, or in other words if no energy is provided to alter it. Once sufficient extra energy is provided into the system, the superheated fluid becomes vapor and creates acoustic noise. To protect the superheated fluid from environmental contamination a gel is used in PICASSO bubble detectors. The gel protects each droplet from environmental change. It also encases the droplets so that imperfections on the surface of the detector walls will not initiate spontaneous bubble formation. The PICASSO experiment uses millions of small sensitive droplets of C_4F_{10} with diameters of 50-200 micrometers loaded inside a gel of polymerized liquid, where the total mass of these droplets is about 60 to 110 grams in each detector [6]. The boiling point for these droplets is T_b = -1.7^oC at a pressure of 1.013 bars. These droplets are continuously active, however if too many droplets within a detector evaporate the gel can be damaged. Every 40 hours the detector is therefore put under pressure so that the gas bubbles transform back to liquid droplets.

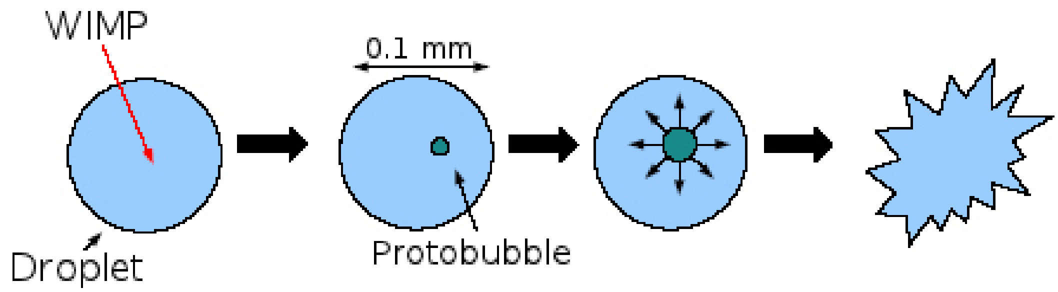

Figure 3.1: If a dark matter particle hits a nucleus in a tiny superheated droplet, the atom recoils and deposits its energy as a heat spike, which in turn triggers a phase transition [41].

In PICASSO, when a WIMP hits a fluorine atom in a droplet (Figure 3.1), energy is transferred to the fluorine atom and the atom deposits its kinetic energy to the droplet. For the phase transition to occur in a superheated liquid a critical minimum amount of energy, E_c, has to be supplied within a volume of critical radius R_c, then it grows explosively until all of the liquid evaporates into a vapor bubble. Both the critical energy and critical volume are dependent on the local temperature. During the phase transition acoustic energy is released. The detection principle can be understood as receiving an acoustic signal from a particle interaction, that is causing a phase transition. The explosion creates an acoustic pulse (Figure 3.2); sound is transferred to the walls of the acrylic tube where piezo electric sensors pick up the signal and send an electronic signal to the computer [5].

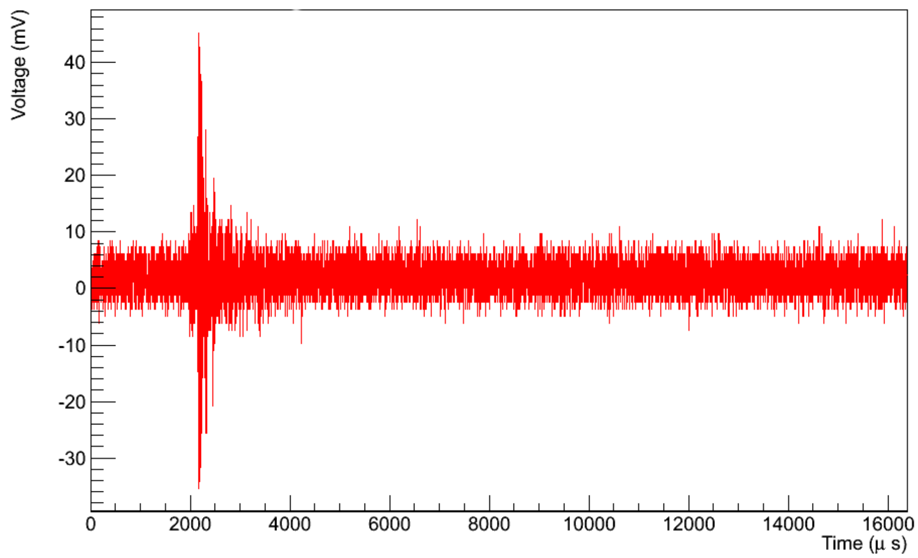

Figure 3.2: This mini-explosion gives an acoustic signal lasting about 4 milliseconds and can be recorded easily with piezoelectric transducers [41].

The operating temperature of the detectors is controlled with a precision of 0.1^{o}C. Most of the calibration runs are done at temperatures between 20^oC and 50^oC. The detectors can be made insensitive to low deposited energy densities by controlling the temperature and pressure. There are several steps of analysis performed to analyze the data which will be described in the following chapters.

3.B Detector Geometry

The experiment is located at SNOLAB, 2km underground inside a cylindrically shaped clean room. The PICASSO installation is about 2.2 meters high, 2 meters long and 2 meters wide (Figure 3.4), it accommodates 32 detectors.

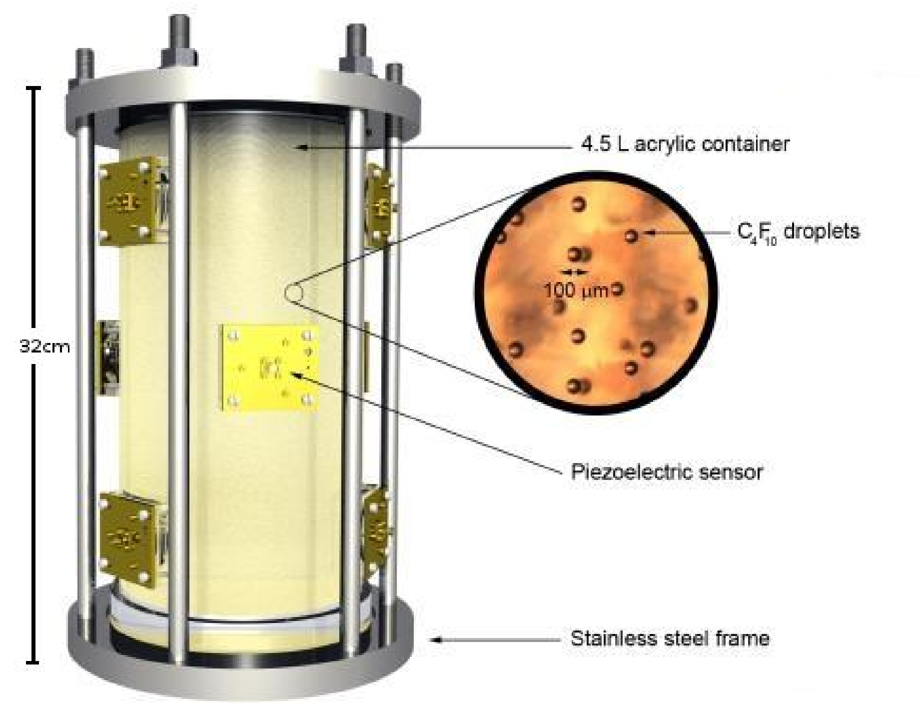

Figure 3.3: Shown here is one of 32 detectors used by PICASSO installed at SNOLAB. It is a 4.5 L module with about 80g of active mass of C_4F_{10}. Droplets are suspended in an elastic polymer. Signals are recorded by 9 piezo electric sensors [41].

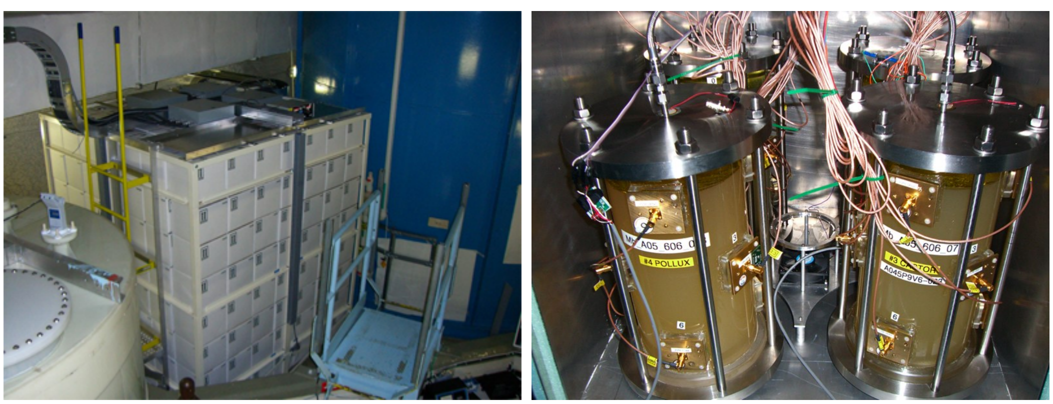

Figure 3.4: A picture of the PICASSO experiment installed at SNOLAB and a picture of the inner part of a TPCS where 4 detectors are placed [41].

A detector(Figure 3.3) is filled with polymerized gel and dispersed superheated droplets inside the gel. A group of four detectors is installed in each of

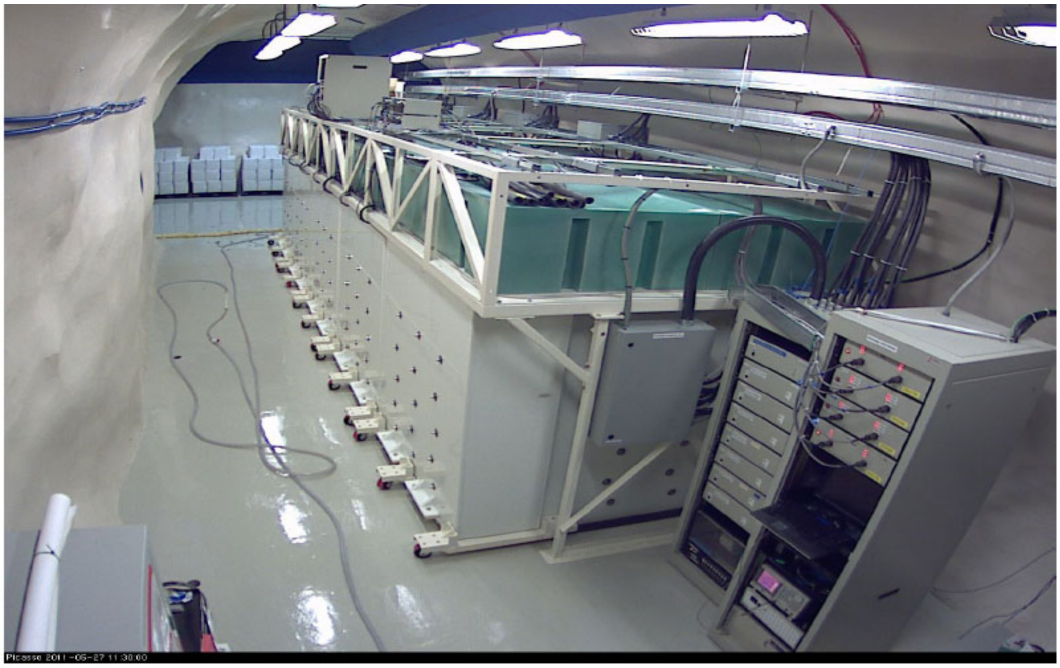

Figure 3.5: An image of the new PICASSO setup.

the 8 thermally and acoustically insulated boxes called TPCS (Temperature and Pressure Control System). Detectors consist of cylindrical modules of 14 cm diameter and 32 cm height, the containers are fabricated from acrylic and are closed on top by stainless steel lids sealed with polyurethane O-rings [6]. The cylindrical acrylic containers are filled with liquid that contains 4.5 liters of cesium chloride gel in solution (salty detectors) or polymerized acrylamide gel with glycerine and polyethylene glycol as the main ingredients (saltless detectors). In 2007 PICASSO started to collect data using salty detectors. Salty detectors contain more radioactive contaminants mostly from the cesium chloride which can lead to large background. The new saltless detectors were designed to replace the salt in the detectors to remove this background source. In the new installation PICASSO operates only saltless detectors. The gels are loaded with 50-200μm diameter Freon (C_4F_{10}) droplets which are used as active liquid. At the walls of the acrylic cylinders 9 piezo electric sensors are attached, which are connected to a computer with cables to record the acoustic signals from the droplet burst that typically last a few milliseconds. Every four detectors are placed symmetrically inside a 65cm by 65cm by 63cm TPCS (Figure 3.4), a TPCS is an aluminum box covered with foam that does not transfer heat and sound between the inside of the box and the environment. There are two different setups: the utility setup with two levels and the new ladder lab setup with eight TPCSs in a row (Figure 3.5). In 2011 PICASSO moved from the old utility room to the new ladder lab area. At the same time PICASSO changed its shielding from water filled cardboard boxes to new thicker water tanks which absorb more neutrons than the old shielding. The PICASSO setup changed from a two level setup to a linear setup. In the old utility setup there were eight different TPCSs, four boxes in the lower level and four in the upper level, each of them separated by steel plates. The entire installation is surrounded by a water shield which serves as a neutron moderator and absorber. The water shield serves to prevent the fast neutron flux coming from the surrounding rock from entering the experiment. Neutrons that are produced by (α, n) reactions in the rock wall are effectively shielded using materials with abundant hydrogen, like polyethylene or clean water. Such a shield reduces the neutron energy sufficiently so that they cannot cause nuclear recoils above threshold in superheated liquids.

3.C Response to background and discrimination

The PICASSO experiment is also sensitive to background radiation. Cosmic rays, such as muons, rarely reach SNOLAB because of its depth, so for PICASSO the main backgrounds are:

- Neutrons that are produced by (α, n) reactions from the decay of uranium and thorium in rock walls.
- Neutrons from muon spallation of cosmic ray muons. The rate of production of these neutrons is very low at SNOLAB, and they are not considered here.
- Alphas, resulting from the decay of radioactive contaminants in the detector material.
- Gamma rays, the source of which are the surrounding materials, the gel and the aluminum plates of the TPCS.

The detector response to various particle types is shown in Figure 3.6 as a function of temperature between 10^oC and 70^oC.

The detectors are shielded from neutrons using water cubes around the detectors with a shielding efficiency of about 98% [17], which is a good reduction. Alpha particles are the second main background, fortunately, they can be distinguished from WIMPs [4]. Alphas and neutrons can be discriminated based on their acoustic signals. Alphas signals are larger than neutron signals, this can be explained by a single phase transition only of droplets for neutron interactions and many phase transitions for alpha hits. However, in practice

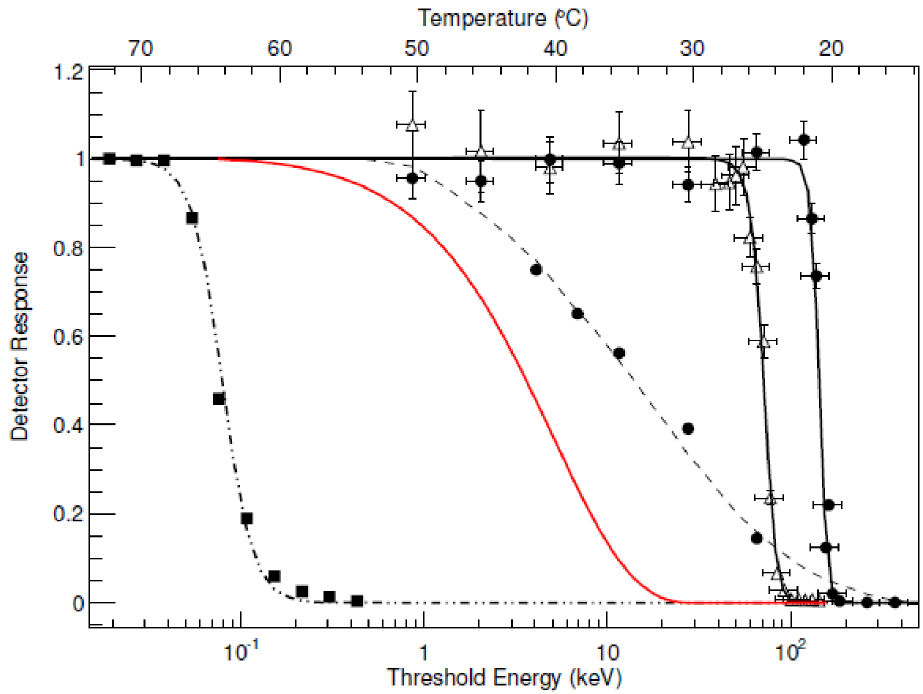

Figure 3.6: Normalized detector response to certain particles as a function of temperature. Response to different kinds of particles in superheated C_4F_{10}. From left to right: 1.75 MeV γ-rays and minimum ionizing particles (dot-dashed); ^{19}F recoils modeled assuming the scattering of a 50 GeV/c^2 WIMP (red); poly-energetic neutrons from an AcBe source (dotted); particles at the Bragg peak from ^{241}Am decays (open triangles); and ^{210}Pb recoil nuclei from ^{226}Ra spikes (full dots) [4].

only about 80% of alpha signals can be discriminated at the moment, due to a limitation of the acoustic readout of the detectors. The task of discriminating all alphas from the data is under development. The other background for PICASSO is gamma rays. Gammas are undetectable at temperatures below 55^oC, since at low temperature gammas do not provide sufficient energy to droplets to initiate a phase transition [7].

3.D Why PICASSO is located at SNOLAB

The experiment is located at SNOLAB 2km underground in order to keep the detectors protected from cosmic rays. Experiments intending to detect dark matter by direct detection rely on detector technologies capable of detecting energy thresholds well below 100 keV in order to observe recoils induced by a WIMP scattering off a nucleus. In order to have sufficient sensitivity to a corresponding WIMP cross-section [23], such detectors must also be constructed of materials with extremely low levels of natural radioactivity and be able to discriminate background (ionizing rays and electrons) that can produce a potential WIMP signal. Next to this discrimination dark matter search experiments have to reduce nuclear recoil events from neutrons to almost zero, otherwise they will not be able to discriminate WIMP recoils from neutron recoils. In order to reduce the nuclear background events, most dark matter search experiments are located in underground observatories. In addition they cover the detectors with materials that are rich in hydrogen to shield the detectors from fast neutrons. Two classes of particles are distinguished that disturb the detectors:

1. Neutrons produced by muons traversing the detectors.

2. Neutrons created in the external rock by muons or α - n reactions.

The production of fast neutrons depends strongly on the depth and composition of an underground site. Or in other words, the neutron production rate at large depths due to muons is two to three orders of magnitude smaller than that of neutrons arising from local radioactivity through (α, n) reactions, which means as the depth of the underground site increases, the cosmic-ray muon flux decreases. The muon-induced neutrons have a very hard energy spectrum extending to several GeV and can penetrate to significant depth both in the surrounding rock and detector shielding materials, which is really significant to dark matter experiments. In Figure 3.7 the cosmic-ray muon flux and muon-induced fast neutron flux as a function of depth for specific existing underground laboratories around the globe [23] are shown.

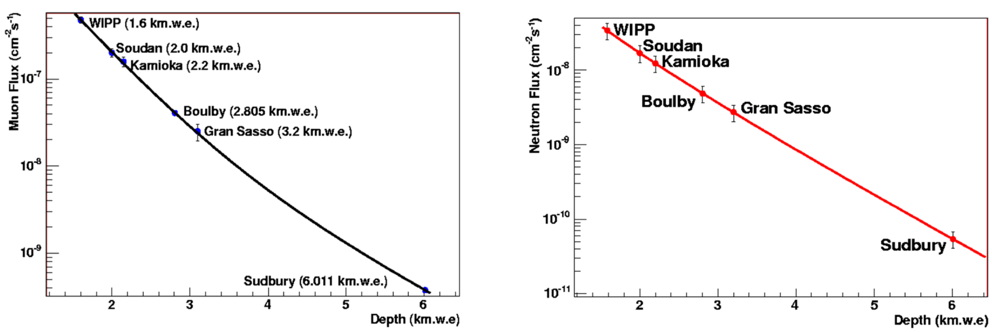

Figure 3.7: In the first plot the cosmic-ray muon flux and in the second the muon-induced fast neutron flux as a function of depth (kilometers water equivalent) for specific existing underground laboratories around the globe are shown [23].

As seen from the plots SNOLAB at Sudbury has a low cosmic-ray flux and fast neutron flux, thus a detector operated at SNOLAB has the lowest rate of background events compared to all other underground labaratories around the world. This is the reason to establish PICASSO at SNOLAB.

3.E Recent PICASSO results

The work done from 2008 to 2011 is presented in the recent paper that was published in the beginning of 2012. The recent results were obtained using 10 detectors with a total target mass of 0.72 kg of fluorine and an exposure of 114 kg days. The main improvements with respect to results published in 2009 are: a reduction in alpha background by up to a factor eight, use of a new discrimination method which allows discrimination of non-particle induced events and the extension of the analysis from 2 to 10 detectors. However,

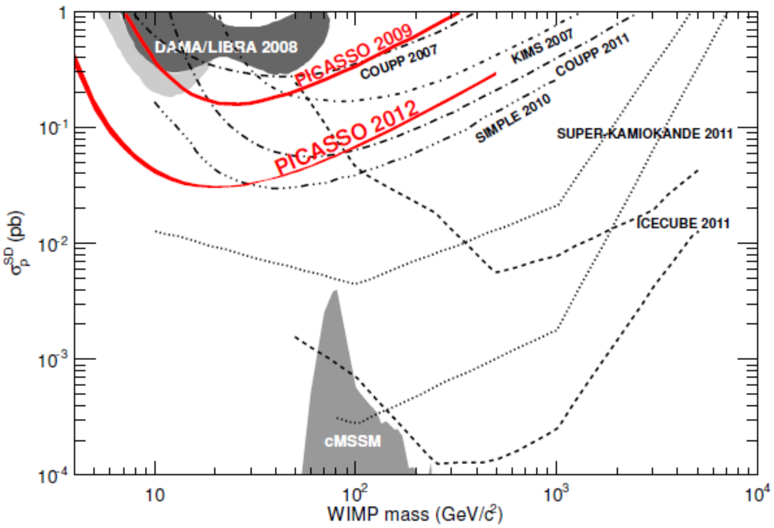

Figure 3.8: Upper limits at 90% C.L. on spin dependent WIMP-proton interactions. PICASSO limits are shown as full lines [4].

the origin of the alpha background is still uncertain and under investigation. Events were normalized with respect to the active mass (^{19}F) and data taking time for all temperatures. No dark matter signal was found. For the spin dependent sector, where the scattering of dark matter on ^{19}F is dominated by interactions with protons, the best exclusion limits were obtained for WIMP masses of 20 GeV/c^2 with a cross-section of 0.032 pb (90% C.L.) [4]. The resulting exclusion curves for the WIMP cross-section on protons as a function of WIMP mass are shown in Figure 3.8.

Chapter 4

SIMULATION OF PICASSO EXPERIMENT AND STUDY OF THE SHIELDING EFFICIENCY

4.A PICASSO Neutron Calibration

To detect WIMPs using the superheated liquid technique it is important to discriminate events from WIMP-nucleon interations from all other types of events. For instance, gamma particles create Compton electrons, WIMP and neutron particles produce nuclear recoils. Fortunately, signals from electrons differ from signals from nuclear recoils. The interaction of energetic neutrons is similar to that expected from WIMPs, that makes them produce a similar acoustic signal. Since the aim of dark matter search experiments is to detect the WIMP, one needs a signal similar to that which would be produced by

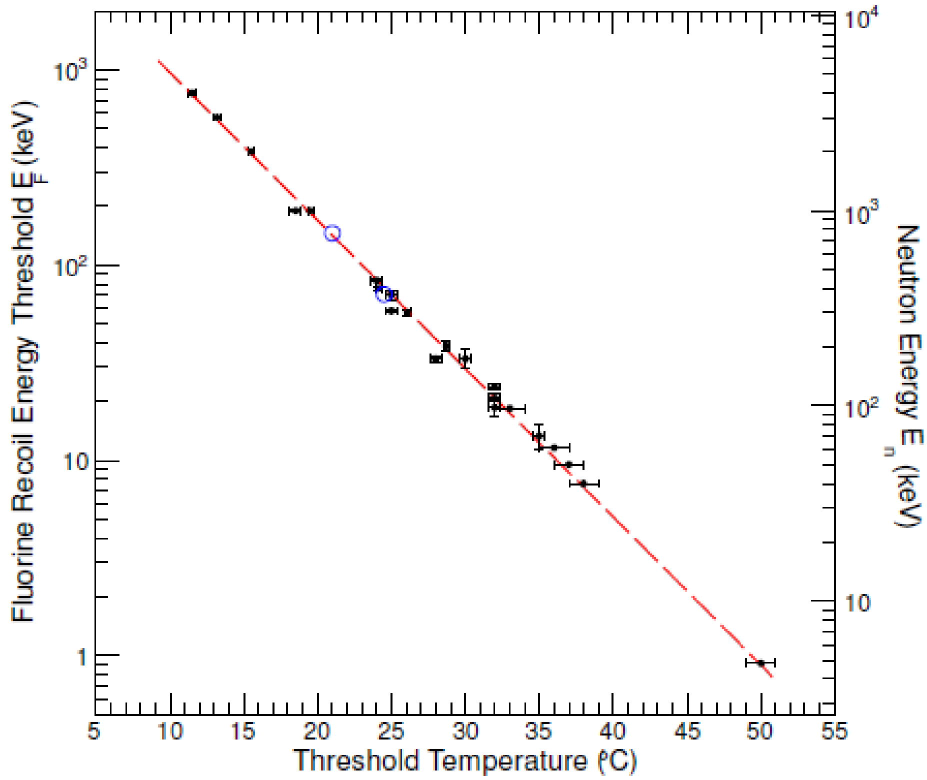

Figure 4.1: Relationship between the energies of mono-energetic neutrons (right vertical scale) and the maximum recoil energy of fluorine (left vertical scale) with the temperature measured at the threshold [4].

a WIMP to calibrate the detectors. PICASSO uses neutrons to learn more about the detector response. When a detector is built it is tested before use and this test is done with neutron particles. Moreover, calibration with neutrons permits one to determine the response curve predicted for WIMPs. Neutron calibrations are also used to study the response of PICASSO detectors to different source locations. For this purpose, extensive calibrations are performed with neutrons in PICASSO. In most neutron calibrations PICASSO uses an americium beryllium (AmBe) source that emits about 70 neutrons per second with energies up to 12MeV. In PICASSO, a neutron calibration data taking run typically lasts for 2-4 hours after which the detectors are recompressed at a pressure of 6 bar in order to reduce bubbles to droplets and to prevent excessive bubble growth which could damage the polymer gel. Neutron calibrations are also performed to study the sensitivity of detectors at different temperatures. For WIMP searches it is important to know the minimum nuclear recoil energy that produces a bubble as a function of temperature. Neutrons scatter elastically off the nucleus, the threshold recoil energy (at 1 bar) as a function of temperature is given by:

$$E_{th}^{F} = 0.19E_{th}^{n} = (4.93 \pm 0.15) \times 10^{3}(\exp(-0.173 \cdot T(^{0}C)))(keV) \qquad (4.1)$$

where the factor of 0.19 represents the maximum fraction of the energy of the incident neutron E_n transmitted to the nucleus, and E_n is the energy of incoming neutrons [4]. According to the temperature range of operation in PICASSO, and in case of ^{19}F recoils this translates into a range of sensitivity from E_{th}^{F} >2.0 keV at $45^{o}C$ to E_{th}^{F} >200 keV at $18.5^{o}C$. Figure 4.1 shows measured rates for detectors which are lined up with a straight line fit, which shows that PICASSO bubble detectors are well understood. Another fact about this Figure is that at a temperature of $50^{o}C$ the threshold energy for fluorine recoils is about 1 keV. This is the lowest calibrated threshold of any dark matter search experiment in the world. Since the detector response to different neutron energies is known, it is possible to predict the detector sensitivity to different WIMP energies.

4.B Overview of the PICASSO Monte Carlo Code

4.B.1 Geant4

Geant4 (GEometry ANd Tracking) is a toolkit for the simulation of the passage of particles through matter using the Monte Carlo (MC) simulation method. It is software written using the C++ computer language and developed by a collaboration at CERN [39], [2], [1]. The software is used to simulate particle behaviour inside a medium. The areas of Geant4 application include high energy, nuclear, accelerator physics and space, and medical science. The software is used by a number of research groups around the world. In this research project the Geant4 simulation toolkit was used in order to study the PICASSO detector response to neutrons. All the MC simulation results in this document were performed using Geant4 9.5 $2^{nd} release$ (December 2011).

4.B.2 Old PICASSO setup geometry

The PICASSO setup was modelled at the center of a cylindrical room. The setup is shown in Figure 4.2. The installation is located at the center of a horizonatal cylindrical room with a diameter of 7.5m and length of 30m, on the top and bottom the wall is about 2.5m away from the setup, on the right and left the wall is about 14m away from the left and right sides of the volume.

The simulated geometry of PICASSO in the Geant4 code is almost the same as the geometry of PICASSO at SNOLAB with only a few assumptions. All 32 detectors are located at their nominal places. On the outer part of the TPCSs are aluminum sheets, on the outer side of the aluminum box is foam,

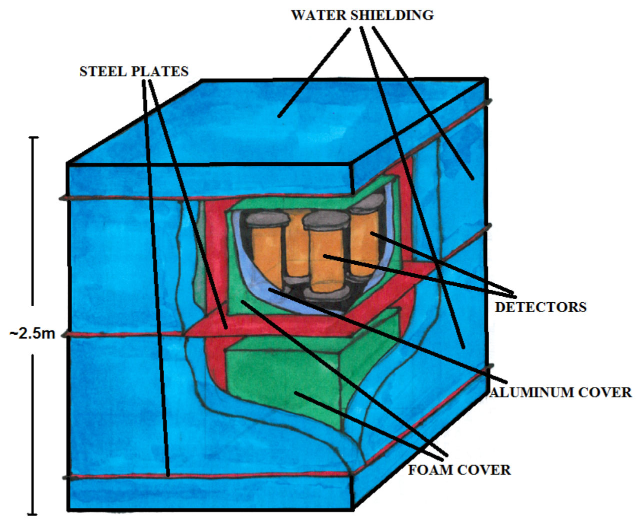

Figure 4.2: Image of a PICASSO setup as in put into the Geant4 simulation.

with the same thickness as in PICASSO. All the TPCSs are located in their individual rooms that are separated with aluminum plates and water cubes for shielding around the steel frame. The sizes and the thicknesses are equal to that in PICASSO; however the water cubes are assumed to have 25% of paper and 75% water mixed equally. The second assumption of the geometry is that the wires and electronics inside the TPCSs. Every time a detector is accessed, the wires are moved from their places and it is impossible to code all the wires and their locations. Instead of designing all the electronic parts individually these materials were mixed according to weight in the air surrounding the detectors. The air mixture is filled gas inside the aluminum box, with 80% of air, 10% of steel and 6% of plastic and 4% of copper by volume. According to the latest data collection run, there are 15 saltless, 1 freonless and 16 salty detectors. The simulation has the same distribution of detectors. A model of a detector in the code is shown in Figure 4.3. The assumption is that 1% of the total mass of a salty gel is a C_4F_{10}, which made all detectors to have the same amount of active mass, which is 77.8 grams.

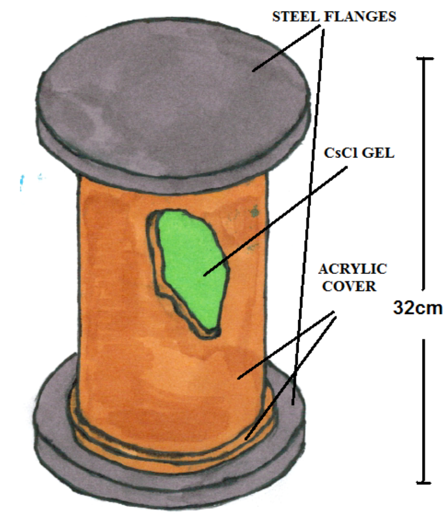

Figure 4.3: Image of a PICASSO bubble detector as in put into the Geant4 simulation. Rods and piezos around the detectors are mixed in with the air surrounding the detectors.

4.B.3 Description of the new Installation

The geometry of the new PICASSO setup in Geant4 is the same as it is in reality. There are 8 TPCSs placed one after another so that they line up in a straight line, where only detectors from TPCS 1, 2 and 7 are in operation at the moment (October 2012). Detectors and TPCSs are the same as in the old setup. The water tanks that are used to shield the detectors are 50 cm thick, where the old water cubes were only 30 cm thick. There are 12 saltless detectors, 4 in each TPCS with an active mass of 77.8g each.

4.B.4 Simulated Physics

The code of the simulation has to describe the construction and geometry of the experiment and all physics processes represent the experiment. In the code all types of particles and all types of neutron physics processes, like neutron capture, neutron elastic and inelastic interactions, are simulated. However, in some Monte Carlo studies only the elastic neutron interaction process was used and all other processes were switched off since the contribution of other processes compared to elastic neutron interaction is small.

4.B.5 Event simulation

For each elastic interaction of neutrons with the fluorine inside any of 32 detectors (for the old setup) and 12 detectors (for the new setup), the neutron energy, position and secondary particles that were created were recorded. Each detector inside the PICASSO setups is sensitive to neutrons with energies higher than a threshold energy which is assigned according to the temperature of the run. If a neutron entering a certain detector creates a fluorine recoil it was counted as an event. Most of the nuclear recoils take place in hydrogen-rich media, such as water, since the neutron cross-section of hydrogen is large. Neutrons loose their kinetic energy very quickly and cannot cause a bubble when they have lower energy than the threshold energy of a detector. The code was modified to kill the tracks of neutrons and their secondaries when the neutron energy is too small to be considered.

4.C Analysis and Simulation of Neutrons Coming from the Rock for the old setup

At the location of the experiment, a depth of 2070 m, 90% of the fast neutrons above 5 keV are produced by (α,n) reactions in the surrounding norite rock, with the remaining 10% being fission neutrons from radioactive heavy elements found in the rock. In order to estimate the expected neutron flux reduction by the shielding, and to test the accuracy of the Geant4 code, Monte-Carlo (MC) simulations have been performed. The purpose is to study neutron background from the rock and the efficiency of the water shielding using two different initial neutron spectra. Neutron flux and spectra from the mine rock have been calculated using Monte Carlo simulations. Spectra of neutron events inside the setup and at the detectors are plotted. In this chapter the plots show the spectra of neutrons interacting with gel, not with fluorine. The loading of fluorine is 0.7% in the gel, therefore it would take about 143 neutrons to create 1 fluorine recoil. Therefore the time to produce spectra of neutrons interacting with fluorine would increase by a factor of 143.For this simulation 32 salty (CsCl) detectors with an active mass of 77.8g each were used.

4.C.1 Neutron spectra

Neutron Spectrum #1

Neutrons are produced by (α, n) reactions from α decay in the uranium and thorium decay chains in the rock walls of SNOLAB and by spallation caused by muons passing through the rock. According to a measurement done by the SNO collaboration the flux of neutrons coming from the walls of the room is

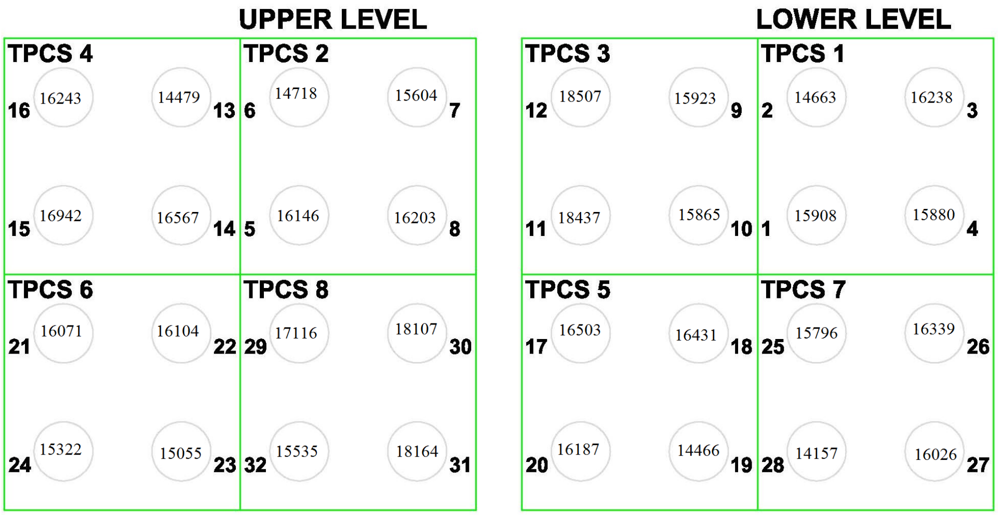

Figure 4.4: Number of neutron recoils off gel inside detectors out of 1.34×10^7 neutrons entered.

5000 neutrons per square meter per day with the energy range of 0-10MeV. To get an upper limit of the neutron flux in the shield a flat spectrum is assumed. This serves as worst case scenario to give an upper limit of background efficiency. For this MC simulation the assigned threshold energy is 26keV which corresponds to temperature, T=40^oC. All neutrons with energies below 10keV were killed, since the detectors are not sensitive to neutrons with energies lower than 10keV at 40^oC. From the surface of the cylindrical room about 3.97×10^8 neutrons are expected to enter the room in 100 days. Out of 3.97×10^8 neutrons shot in random directions from the surface of the walls 1.34×10^7 neutrons are seen at the PICASSO setup before they go through the shielding. In Figure 5.1 the total number of neutrons recoiled in each detector (neutrons that interacted with the gel, not only with fluorine) was presented. Out of 1.34×10^7 neutrons that enter the setup 5.16×10^5 neutrons pass through the shielding. The average number of neutrons interacting with the gel was calculated to be

1.61×10^4 neutrons in 100 days. One can calculate the shielding efficiency to be 96.15±0.05% by not considering neutrons with energies lower than 10keV. The rate of nuclear recoils on fluorine in each detector is calculated to be 0.56±0.02 per day at 40^oC.

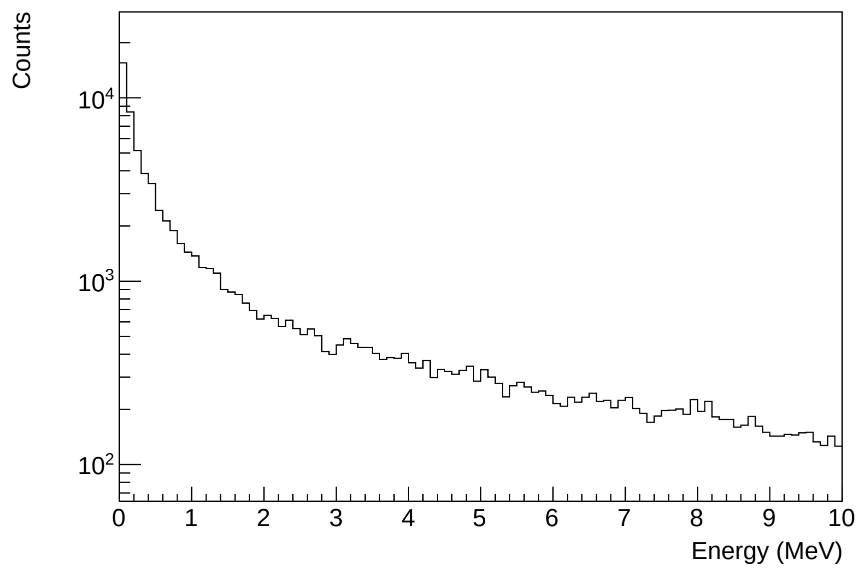

Figure 4.5: The spectrum of neutrons interacting with gel inside the detectors (all 32 detectors combined).

The spectrum in Figure 4.5 is the neutron spectrum at the detectors. It shows the energy distribution of neutrons before interacting with particles inside the gel. All 32 detectors have only slightly different neutron spectra. The mean neutron energy at their recoil inside detectors is 1811.83 keV.

Neutron Spectrum #2

According to the PSTR-11-007 from Alvine Kamaha (Neutron Background Study [17]) neutrons coming from the norite rock are mostly fast neutron with energies between 1 to 10 MeV, but on their way to the lab they pass through

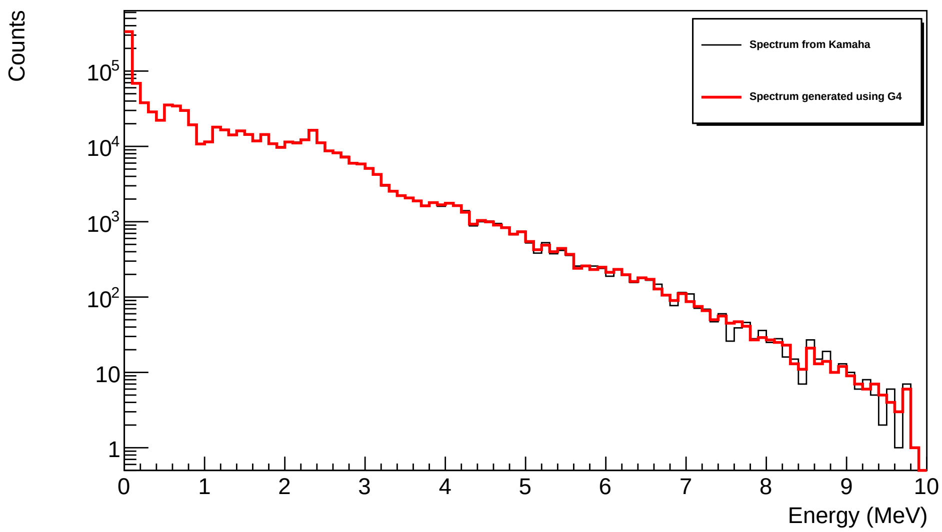

Figure 4.6: Generated Neutron Spectrum using the Geant4 code (red) and the spectrum from Kamaha (black).

about 0.5 meters of rock and get partially thermalized. Kamaha's studies have shown that thermal neutrons inside the lab are dominant and have the energy spectrum as it shown in Figure 4.6 .

Neutrons generated from the spectrum #2 at the surface of the rock will travel through the room, where some of them will escape the room without even coming close to the setup and others entering the setup. Neutrons with energies lower than 0.1keV were killed. The threshold energy was set to 1.91keV which corresponds to a temperature of T=55^{o}C. From 3.5×10^8 neutrons generated which is equivalent to a neutron flux of 88 days, about 9.47×10^6 neutrons enter the volume, 1.71×10^5 neutrons pass through the shielding, out of that number, 3.23×10^4 neutrons are seen inside the detectors and where only 122 neutrons scatter off fluorine. The number of neutron recoils inside the detectors is shown in Figure 4.7. The efficiency of the shielding and the background neutron rate at the detectors are discussed and compared

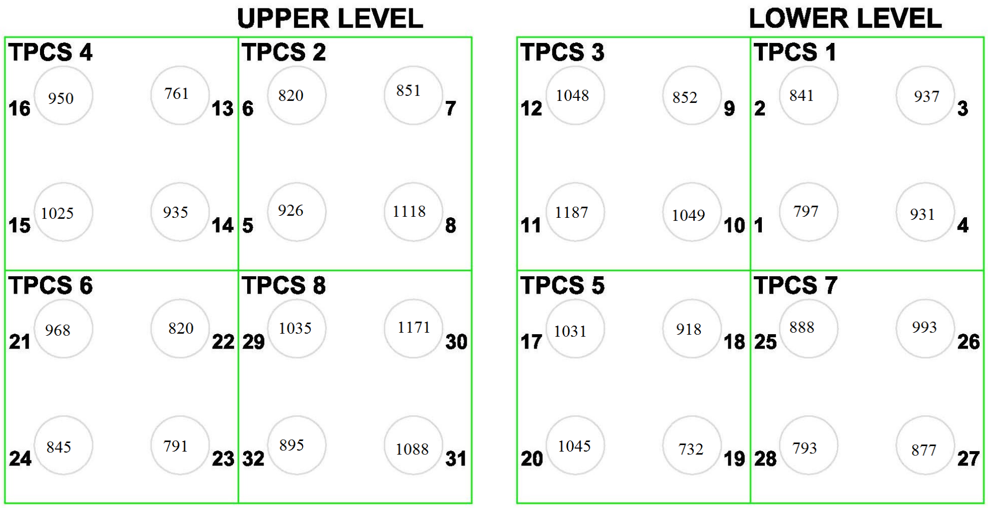

Figure 4.7: Recoiled neutron numbers at the detectors from neutron spectrum #2 out of 8.59×10^6 neutrons entering the volume.

with spectrum #1 in section 4.C.3.

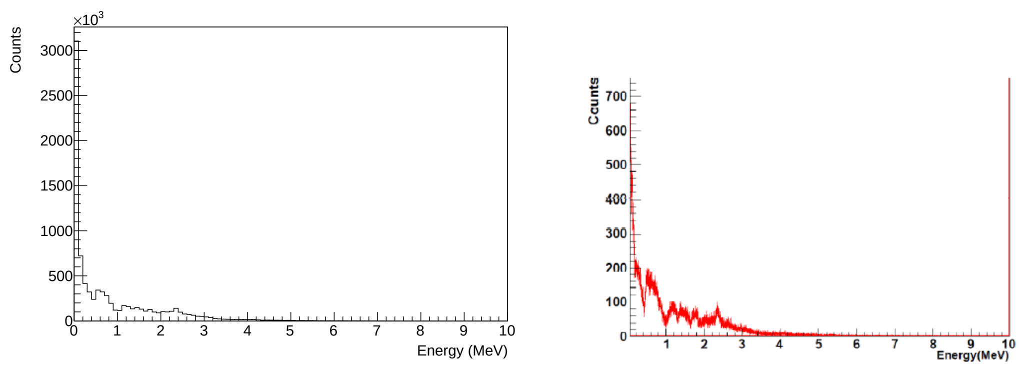

Figure 4.8: Neutron spectra before entering the volume (left: This simulation and right: Kamaha's PSTR)

Neutron spectra outside the shielding and inside the shielding from simulation are displayed next to Kamahas plots from her internal technical report (PSTR) [17], where she has backgroun neutron Geant4 simulation results of only old utility setup. They are similar to each other with small discrepancies,

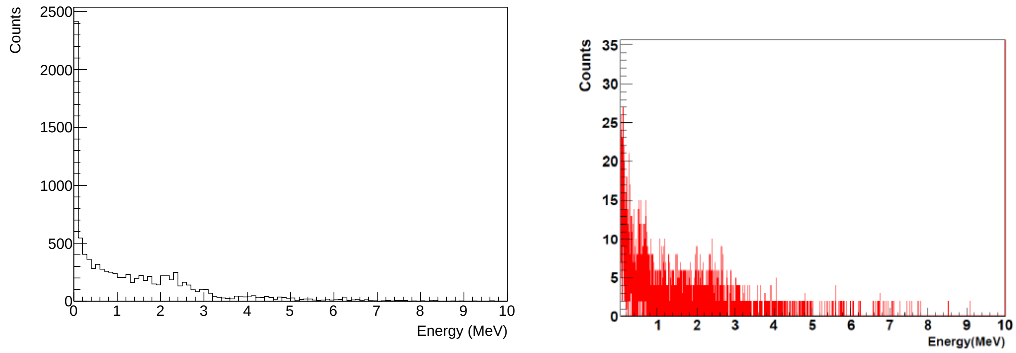

Figure 4.9: Neutron spectra after passing the shielding (left: This simulation and right: Kamahas PSTR)

which might be due to differences in detector geometries. In this geometry the shield is represented as a cardboard/water mix which is neglecting the gaps through which neutrons can enter the shield (see Figure 4.9 right).

4.C.2 Temperature Dependence of External Neutron Rates

PICASSO is a threshold detector and the threshold changes with respect to the temperature. If a neutron that passes through the shielding and creates an event inside a detector that has an energy higher than 1.91keV, the energy of the neutron is recorded. The number of neutrons with energies above a certain threshold energy for a specific temperature was counted, the same procedure was performed for all thresholds. As a result, a rate against temperature was plotted for both spectra, which is shown in Figure 4.10. Both spectra were used in order to compare the detector response to different spectra at different temperatures. The relative rate corresponds to the total number of fluorine recoils in all 32 detectors at a certain temperature divided by the total number

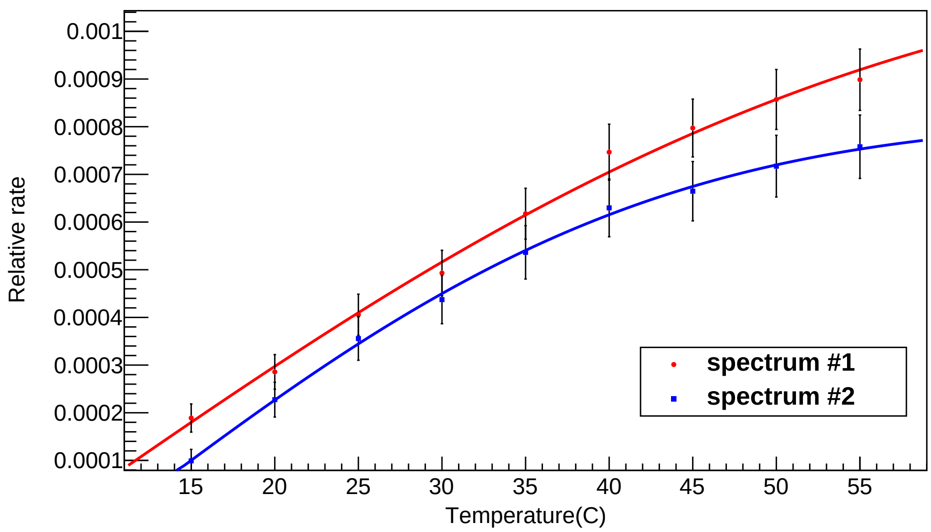

Figure 4.10: Temperature dependence of Background Neutron events. Red line is for spectrum #1 and blue line is for spectrum #2.

of neutrons passed through the shielding.

4.C.3 Efficiency of the shielding and background rate in detectors from both spectra

In order to compare the efficiency of the shielding and the rate in the detectors for both spectra a different simulation was performed, where T=55^oC, E^n_{th}=1.91keV, neutrons that have an energy below 0.1keV were killed. The simulations results are shown in Table 4.1.

In conclusion, the total background neutron rate varies between 0.043±0.002 and 0.69±0.02 per day per detector for spectrum #2 and spectrum #1, respectively. These rates are considered reasonable since in spectrum #2 there are more thermal neutrons than neutrons with high energies. The shielding efficiency is 82.21% and 98.2% for spectrum #1 and spectrum #2, respectively,

Simulation results		
	Using spectrum #1	Using spectrum #2
Neutrons that enter the PICASSO shield	3.48% of all generated	2.7% of all generated
Neutrons that pass through the shielding	0.62% of all generated, 17.78% of all entered the shield	0.05% of all generated, 1.8% of all entered the shield
Neutrons that interacted with fluorine	5.57×10^{-4}% of generated, 0.016% of all entered the shield, 0.09% of all passed through the shielding	3.48×10^{-5}% of all generated, 1.3×10^{-3}% of all entered the shield, 0.07% of all passed through the shielding
Shielding efficiency	82.21% of neutrons are shielded by water	98.2% of neutrons are shielded by water
Background neutron rate	0.69±0.02 per day per detector	0.043±0.002 per day per detector

Table 4.1: Shielding efficiency and detector response to neutrons from the wall rock for the old setup.

where Kamaha's shielding efficiency was 96.86% [17] using spectrum #2, the different discrepancy is due to the differences in geometry of the setup. Another reason is the shape of the room where the experiment is located. The simulation by Kamaha uses neutron inelastic and elastic scatterings, while my simulation uses only neutron elastic scatterings. The performance of the MC simulation was checked against measurements and was in agreement.

4.D New installation shielding efficiency

Using spectrum # 2, the efficiency of the new water tanks used for the new installation was tested. For this simulation the temperature was set to T=55^oC, where E^n_{th}=1.91keV and neutrons that have energy below 0.1keV were killed. The shielding efficiency and detector response results from the simulation are shown in Table 4.2.

Simulation results using spectrum # 2	
Neutrons that enter the PICASSO shield	9.8% of all neutrons generated
Neutrons that pass through the shielding	6.5×10^{-3}% of all neutrons generated and 0.07% of all neutrons entered PICASSO
Neutrons that interacted with fluorine	3.3×10^{-5}% of all neutrons entered PICASSO and 0.05% of all neutrons passed through the shielding
Shielding efficinecy	99.93% of neutrons are shielded by water
Background neutron rate	0.004 ± 0.0001 per day per detector at 55^oC

Table 4.2: Shielding efficiency and detector response to neutrons from the wall rock for the new setup.

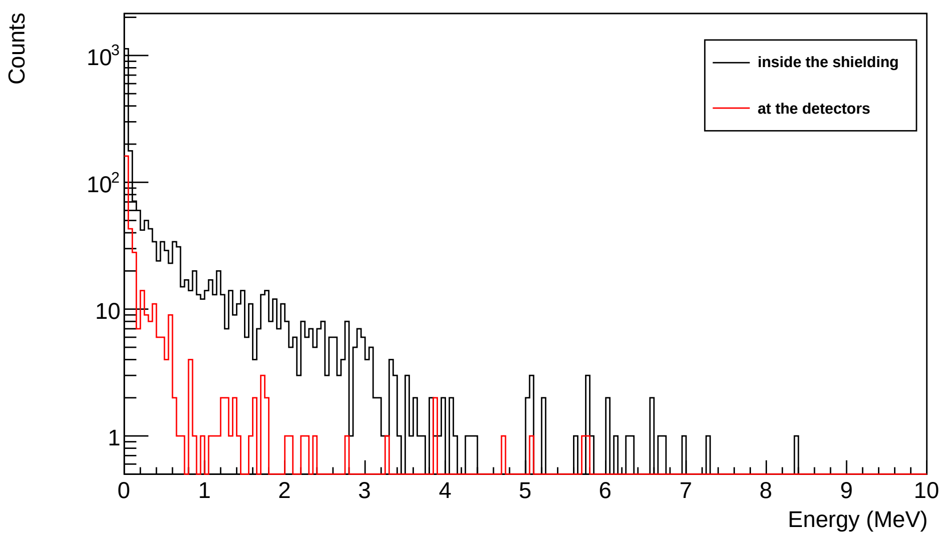

Figure 4.11: Spectrum of neutrons going through the water tanks (black) and spectrum of neutrons interacting with gel at detectors (red) in the new installation.

The efficiency of new shielding is found to be 99.93%, where the one from Kamaha's PSTR is 99.65%. In Figure 4.11 the spectra of neutrons that passed

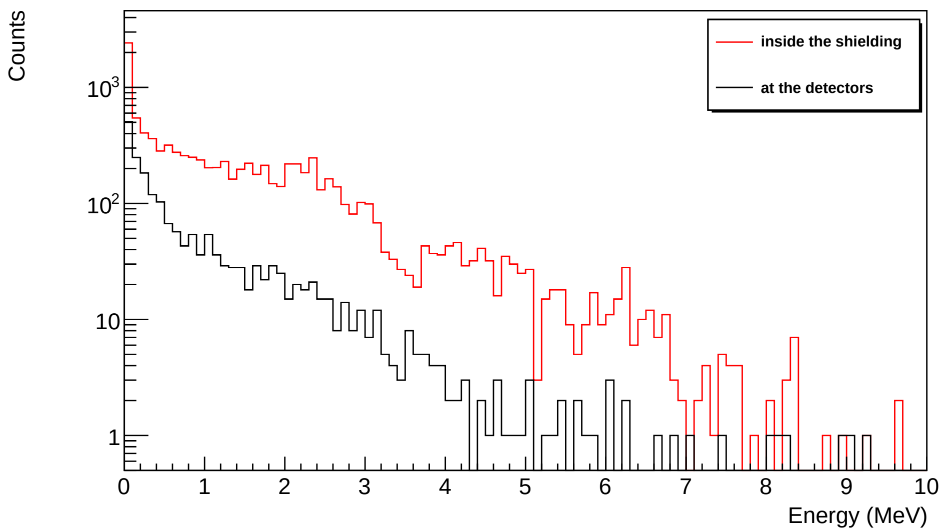

Figure 4.12: Comparison between neutron spectra at the detectors (black) and when they arrive inside the setup (red) for the old setup.

through the water tanks, and of neutrons interacting with gel inside detectors for the new installation are shown. This can be compared to the spectra of neutron particles inside the volume and at the detectors for the old setup which is in Figure 4.12.

Chapter 5

Detector Response and Efficiency Studies

5.A AmBe Neutron Source

The experimental signature of the WIMP is expected to be similar to the signature of the neutron, since the neutron is also a massive neutral particle which creates a nuclear recoil when it interacts with fluorine. Consequently, an AmBe (α,n) neutron source is used to simulate a WIMP source. AmBe (α,n) neutron sources are one of the most commonly used isotropic neutron sources for routine calibration of neutron sensitive devices. The AmBe neutron source spectrum in Figure 5.1 is taken from Kluge and Weise's paper [18]. According to the paper, the neutron energy spectrum of an AmBe (α,n) neutron source was measured by means of a ^{3}He spectrometer in the energy range from 100 keV to 11 MeV.

For the Geant4 simulation of PICASSO the above spectrum was used to simulate the neutron energy spectrum of the emitted neutrons using a modified

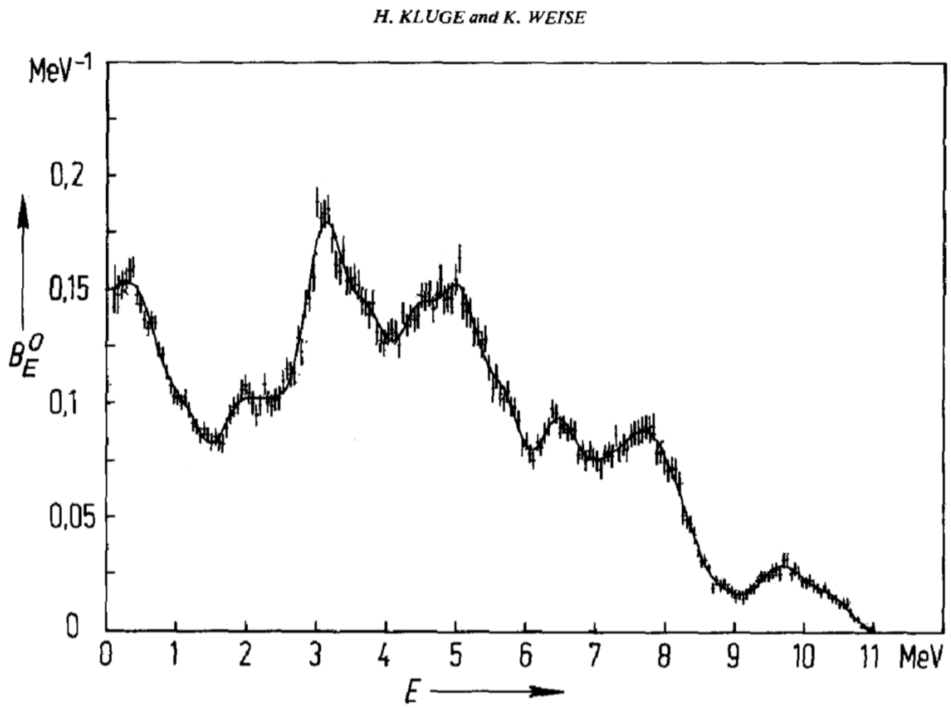

Figure 5.1: Probablity density (B_E) of neutrons (normalized spectral source strength) from $^{241}AmBe$ (α,n) neutron source[18].

Geant4 particle gun. The particle gun stays at the center of each TPCS, it can be moved to different TPCSs based on what is required. The momentum of the neutron emitted from the particle gun is gathered from a random number generator.

The spectrum from Figure 5.1 was divided into 55 sections with a 0.2 MeV bin width. The corresponding probability for each bin was picked, and by using the Acceptance-Rejection Method, and by generating random energies between 0 and 11MeV, the energy distribution from the AmBe neutron source was produced. Neutrons with energies corresponding to the energy value of each bin were generated isotropically with a probability proportional to the height of the bin, the resulting spectrum from the simulation is shown in the red line in Figure 5.2. To study the detector response to neutron particles, two different AmBe neutron source spectra were used, because there was no measurement of the neutron source spectrum of the source used by PICASSO. The second neutron spectrum is shown in black in Figure 5.2. It was taken from the Geant4 "Underground Physics" example, which was taken from [32] and had been modified to use in a G4 example.

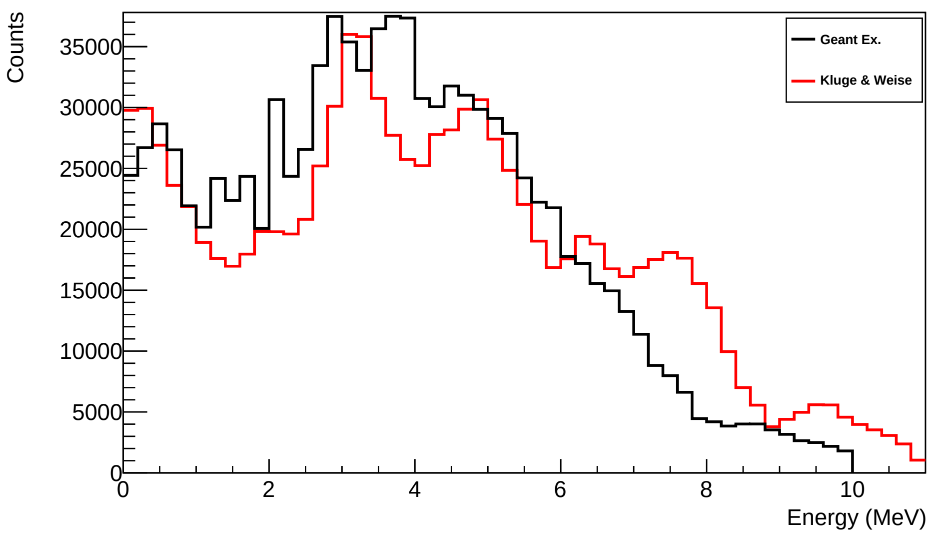

Figure 5.2: The AmBe generated neutron source spectrum from Kluge and Weise's paper [18] (red line) and the AmBe neutron source spectrum from the Geant4 example [32] (black line).

5.B Detector response to AmBe source neutrons

This section presents neutron calibration results from Monte Carlo simulations. Both AmBe neutron source spectra from Figure 5.2 were used to study the detector response. Geant4 was used to study the bubble detector response of the old utility room setup of the PICASSO experiment (2006-2010). The active masses of all detectors were the same and equal to 77.8 g per detector and the source was placed in the center of TPCS #1.

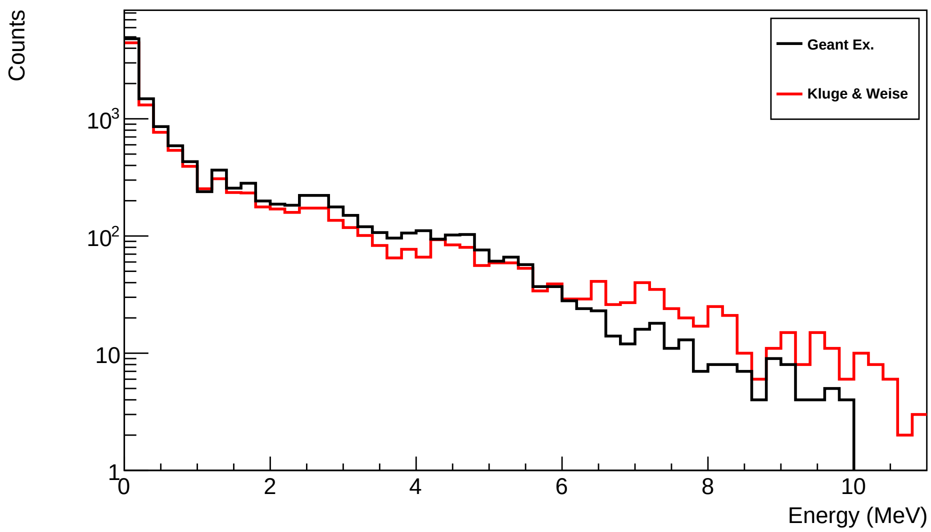

Figure 5.3: Simulated spectrum of neutrons interacting with fluorine of all detectors (red line using source according to [18] and black line using [32]).

The energy of neutrons when they start a nucleation is an interesting subject. In Figure 5.3 the spectrum of neutrons that interacted with fluorine is shown for both AmBe source spectra. This shows how the initial neutron spectra (Figure 5.2) have been changed (into 5.3) while interacting with all materials inside the experiment. Unfortunately, the spectrum of neutrons in empirical data cannot be measured, this is why the spectra of simulated and measured data cannot be directly compared. The difference between energy spectra of recoiled fluorines for both source spectra is shown in Figure 5.4, this is the recoil energies of fluorine atoms after interacting with neutrons.

In order to study the detector response to neutrons as a function of temperature, in the simulation a plot of counts of all events in all detectors as a function of temperature for both AmBe source spectra was created, which is

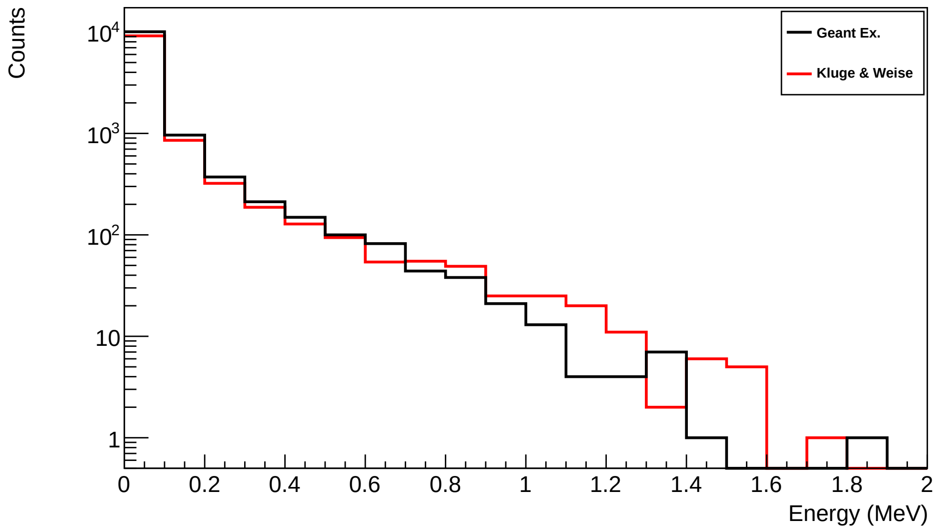

Figure 5.4: Simulated spectrum of recoiled fluorines of all detectors (red line using [18] and black line using [32]).

shown in Figure 5.5. The threshold energy for each temperature was calculated using equation 4.1. The number of counts for each temperature are counted based on the number of events with energies higher than the threshold energy for that specific temperature. As with previous simulations results include only elastic neutron interactions. The curved lines on the graph are fitted error functions. The detector response to neutrons from the AmBe source as a function of temperature will be compared to data in further sections.

The number of recoils in selected detectors from the simulation where the total number of generated particles from the source is 2.4×10^7 which is equivalent to 100 hours of source running, is presented in Table 5.1. It is possible to calculate the rates in each detector using these numbers of recoils. The temperature was set to $40^o C$. Only the closest four and furthest four detectors to the source are shown in the table to compare the rates between them. The distant detectors are expected to have 50-100 times fewer events than the

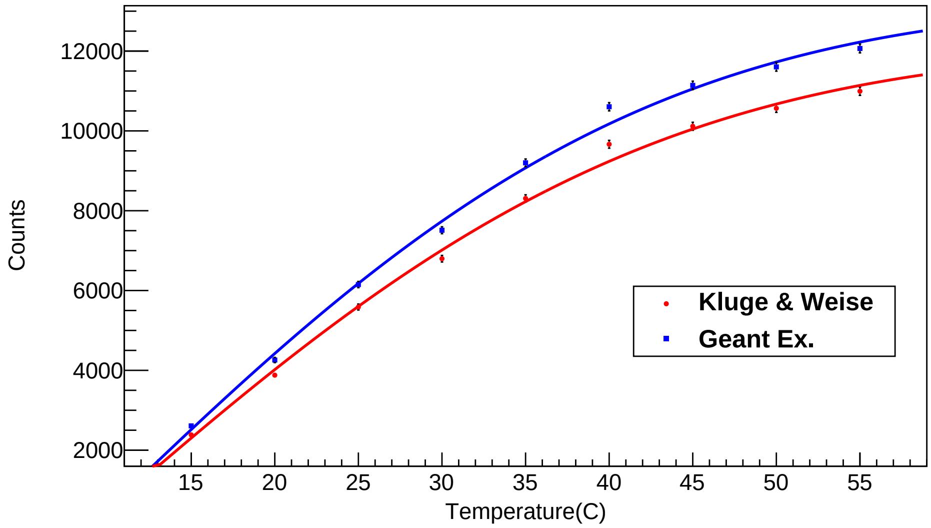

Figure 5.5: Neutron interaction with fluorine as a function of temperature, red dots and black stars are number of events in all detectors from Kluge and Weise's paper [18] and from Geant4 example [32], respectively. Simulation of 32 detectors with the utility room setup.

closest detectors. Rates in the table are calculated using

$$\text{Rate} = \frac{N_d}{t_{total}(s)} \tag{5.1}$$

where N_d is the total number of fluorine recoils and $t_{total}(s)$ is total run length in seconds.

The response of detectors for different temperatures for two AmBe neutron source spectra was introduced. The two different spectra result in difference in detector rates of $\sim$10% at 40^oC

Det.	Kluge and Weise's AmBe source		Underground Physics AmBe source	
#	Counts	Rate (c/h)	Counts	Rate (c/h)
1	17918	179.2±1.3	19097	191.0±1.4
2	18011	180.1±1.3	19220	192.2±1.5
3	18053	180.5±1.4	19058	190.6±1.4
4	17976	179.8±1.3	19083	190.8±1.4
21	243	2.4±0.2	270	2.7±0.2
22	350	3.5±0.2	356	3.6±0.2
23	289	2.9±0.2	235	2.4±0.2
24	188	1.9±0.1	177	1.8±0.1

Table 5.1: Information about rates and efficiencies of detectors from two different sources.

5.C Change in Physics Interactions

To carry out the studies described above only elastic neutron interactions were used, which means only elastic neutron interactions with other materials were simulated. In this section, the difference in the number of recoils when only the elastic process is included and when neutron elastic, inelastic and capture processes are considered in the simulation will be shown. The temperature is set to 55^oC in this study. According to the simulation results, the number of neutron-fluorine recoils from elastic only interactions is 107804±328 and 105092±324 from all neutron interactions out of 2.4×10^7 neutrons generated. The number of emitted events correspond to 100 hours of source running, with Kluge and Weise's AmBe neutron source spectrum. When a neutron interacts elastically it just bounces off a nucleon without energy loss. When it interacts inelastically it scatters off a nucleon, exciting the nucleon, which then emits gamma radiation; sometimes it can emit alpha, neutron or proton radiation. In a neutron capture process, neutrons get absorbed by a nucleus and as a result that nucleus emits gammas, electrons, neutrons, protons, alphas or it just absorbs the neutron and does not emit anything.

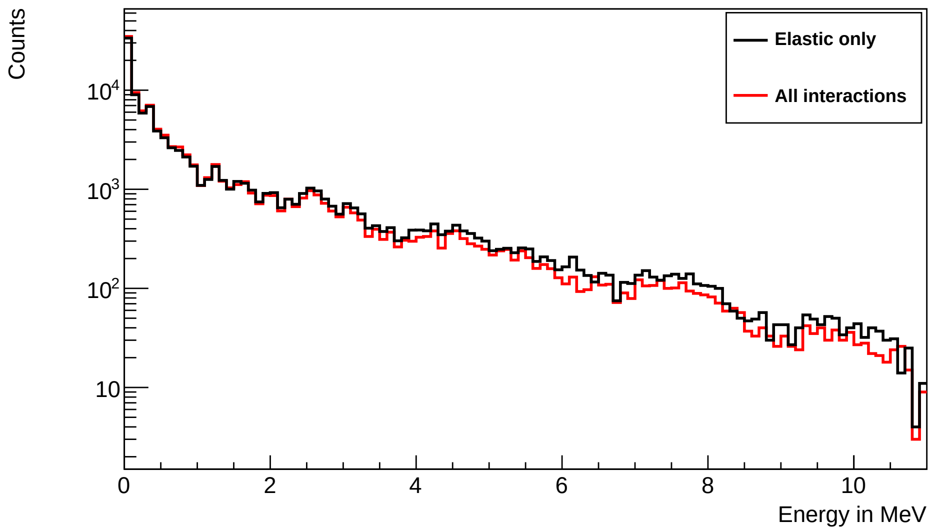

Figure 5.6: Spectra of neutrons for different physics lists using [18].

From the results of the simulation it is clear that the number of neutron-fluorine interactions is larger when only neutron elastic interactions are considered. This basically means that in inelastic interactions neutrons loose more energy than before from inelastic interactions alone and they also get absorbed in the neutron capture process. The number of (n,2n) reactions is determined to be smaller than the number of neutrons that get captured. Luckily, the difference is not large, because the number of bubbles varies only by $(2.5 \pm 0.3)\%$ between elastic interaction only and all interactions. The difference is small and will not change our result significantly at the temperature of interest.

The simulation was performed using two different neutron models, one including inelastic interactions, one without inelastic interactions, they vary between 2-4% at 55^oC. To be sure if the work was right just by using the elastic interactions, the comparison of the spectra of neutrons for both simulation was

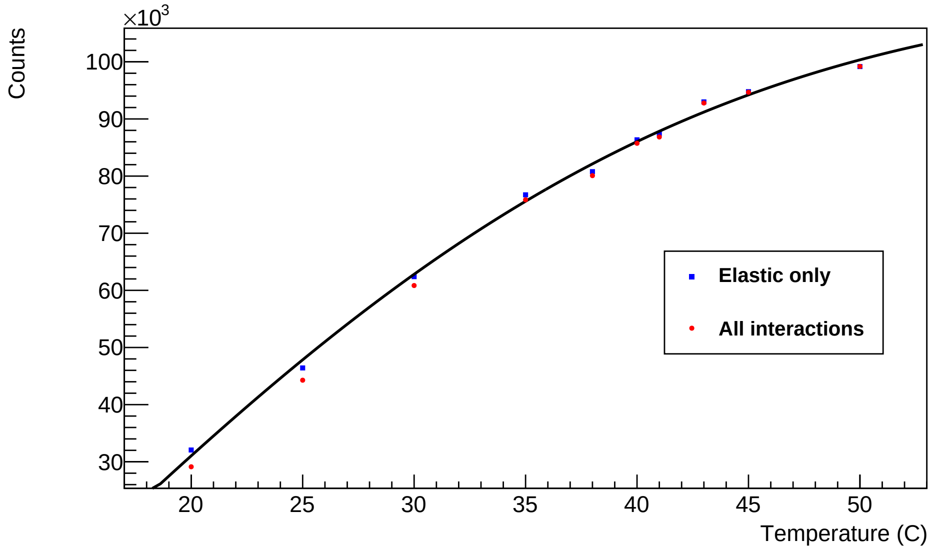

Figure 5.7: Comparison of number of recoils as a function of time for both physics lists using [18].

plotted, which is shown in Figure 5.6. In Figure 5.7 graph which compares the number of recoils as a function of temperature for both physics lists. By looking at the spectrum one can state that the spectra for both simulations are similar to each other, which verifies the work done before by just using the elastic process. Another fact is that the simulation that has all processes takes twice as long to run versus the simulation when only neutron elastic process is considered. In summary, by using only neutron elastic process one can expect reasonable numbers from our simulation which does reflect the reality with a deviation below 5% in a shorter period of time. (This is acceptable because the source spectra uncertainity accounts for a 10% uncertainity.) For low temperatures the deviation is quite significant as can be seen in Figure 5.7, to get an adequate description inelastic interactions should be added for temperatures below $35^o C$.

To compare the simulation and data results of the rate versus temperature, the threshold energy was calculated for each temperature using equation 4.1. To take the energy resolution of the threshold into account a probability that depends on the deposited energy was used: for each temperature, events with energies above threshold were picked up and put into equation 5.2 ([5]) to calculate the probability of an event exploding the droplet. If the probability was larger than the random number generated between 0 and 1 then the event was counted. For this simulation study, elastic and inelastic neutron interactions were switched on, the neutron source was placed in TPCS #1. The delrin cover of the source was also simulated. Both carbon and fluorine recoils were included.

$$P(E_{dep}, E_{th}(T)) = 1 - \exp[\alpha(1 - \frac{E_{dep}}{E_{th}(T)})] \tag{5.2}$$

In the equation the variable α is an unknown parameter which has not been precisely measured yet. Different values for α were used in order to compare the simulation results with the measured data. Simulated neutron calibration rates of detector 72 (old utility setup) from both AmBe spectra as a function of temperature are compared to the experimental data of two different detectors (detector 72 and 131), which is shown in Figure 5.8. Looking at Figure 5.8 one can see that the plot of Underground Physics spectrum is closer to the data graph. In Figure 5.9 the simulated rate of detector 72 from Underground Physics spectrum was compared to the data rate as a function of temperature for various α values.

By looking at the similarity of both simulation and data one can state that the simulation works well for temperature range of 30-45^oC. The discrepancies at low temperatures may be due to an efficiency loss at low temperatures.

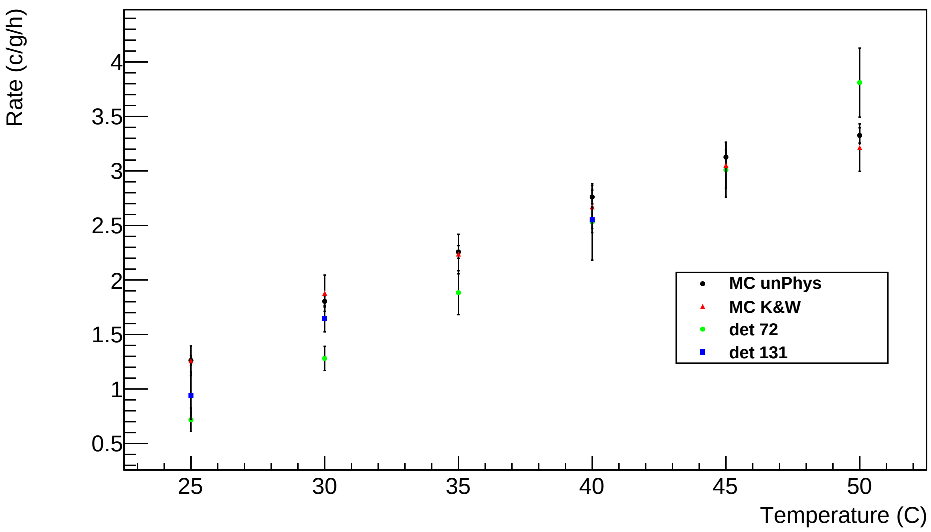

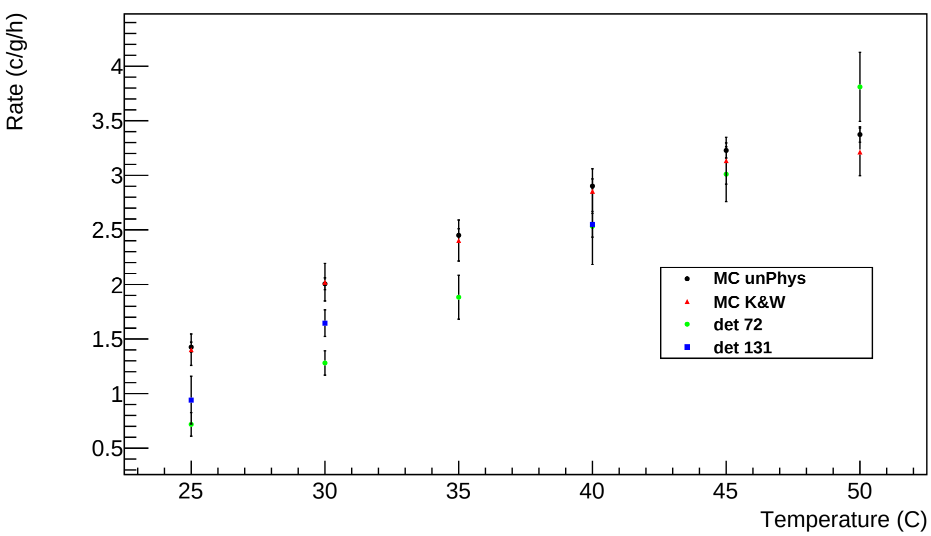

Figure 5.8: Simulated rate as a function of temperature of both AmBe spectra [32], [18] compared to data of detectors 72 and 131 for alpha values of 1.5 and 5.

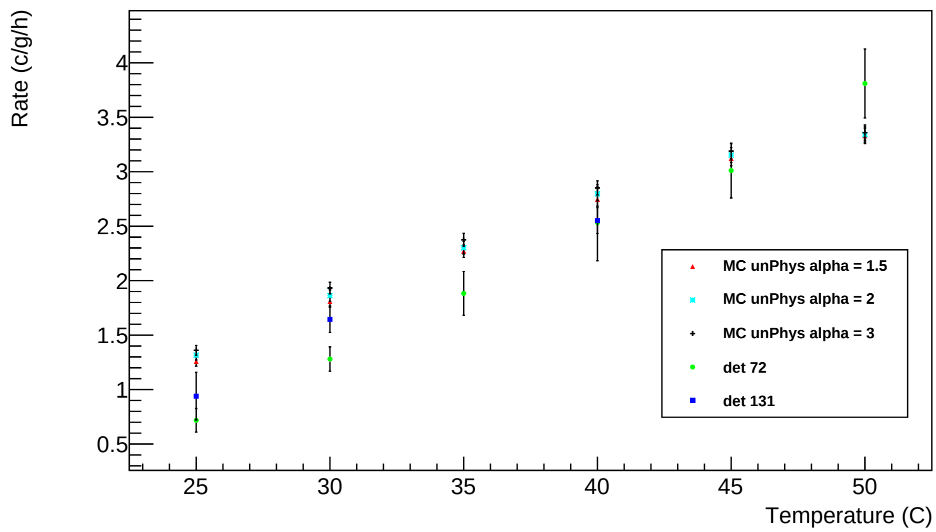

Figure 5.9: Simulated rate as a function of temperature of Underground Physics AmBe spectrum [32] compared to data of detectors 72 and 131.

While at higher temperatures there is more background events in the empirical data. Alpha values that describe the simulation well and fit nicely are in the range between 1 and 3.

Both of the source spectra from the literature do not fully describe the data from our AmBe source. However, the spectral difference seems to be a minor effect compared to the lack of understanding in the α parameter at high temperatures.

5.D Response of detectors as a function of distance

Another interesting subject to study is the detectors response as a function of distance. From the inverse-square law, the neutron flux is inversely proportional to the square of the distance from the source. So, the flux "Φ" of neutrons as they travel distance "d" will decrease to "$\frac{\Phi}{d^2}$". To test if PICASSO detectors respond the same way, another simulation run was performed which is normalized and compared to calibration data. The simulation data were taken with an AmBe source spectrum from Kluge and Weise's paper. The location of the source is in the center of TPCS 1. The number of counts in each detector was normalised with the rates in each detector from the neutron calibration data of two different runs. The resulting plot which is fitted with $\frac{a}{d^2} + b$ function is shown in Figure 5.10.

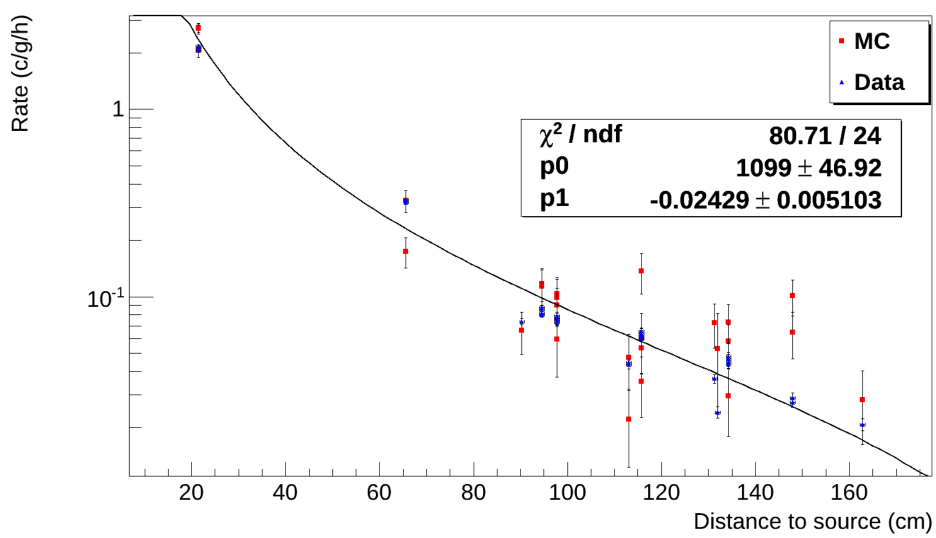

Figure 5.10: Detector response as a function of distance from a source.

The result of the fit was the function $\frac{(1099\pm47)}{d^2} - (0.025\pm0.005)$. The inverse-square law does not totally fit the neutron rates for both simulation and data, which is too simple a fit function for our experiment since the detector medium is not isotropic. One can however use the $\frac{a}{d^2} + b$ function as a guide for the rate over distance relationship of PICASSO detectors. From the comparison of the

Geant4 simulation and empirical data one can see that both simulation and data results deviate significantly from the fitted line, there is an especially large deviation for experimental data. This is mainly caused by some bad detectors (detectors which have electronic problems and which have large backgrounds) inside the setup.

5.E Multiple interactions

A multiple event is defined as a neutron that interacts with fluorine in a detector after making an event in a previous detector. The rate of such interactions is expected to be very small, since the gel is abundant with hydrogen, which reduces the probability of neutrons interacting with fluorine inside the detector medium to a very low level. In this section a simulation of multiple events using Geant4 is described. In a simulation each particle can be tracked, where experimentally it is impossible to track particles. When analysing the data, multiple events are those events which happen in a very short time, in less than $\delta t = 100$ μseconds. The background of multiple events is described here:

- N_s is the total number of neutrons generated or emitted from the source
- N_d is the number of fluorine recoils
- N_m is the number of fluorine recoils in 2 different detectors (multiples)
- $t_{total}(s)$ is the total run time in seconds
- ε_f is the average detector efficiency
- ε_g is the average geometrical efficiency for all detectors

- ε'_g is the average geometrical efficiency after first recoil for all detectors

Of all the neutrons generated inside the source, some will go into the detector and from those that enter a detector some will make a bubble. The number of bubbles created out of all neutrons generated is given by:

$$N_d = N_s \varepsilon_g \varepsilon_f \tag{5.3}$$

Multiple events can be explained as a neutron recoiled in two different detectors.

$$N_m = N_d \varepsilon'_g \varepsilon_f = N_s \varepsilon_g \varepsilon'_g \varepsilon_f \varepsilon_f \tag{5.4}$$

Using these criteria rate and efficiency of detectors are defined as:

- Rate of bubble events: $\frac{N_d}{t_{total}(s)}$
- Net efficiency of detecting a bubble (E_n^f): $\frac{N_d}{N_s}$
- Net efficiency of detecting a multiple event: $\frac{N_m}{N_s}$

5.E.1 Multiple interactions in Neutron Calibration Data

From neutron calibration data the number of multiple events was found to be 98 events in 177.6 hours of source running at 40^oC from data, shown in Table 5.2. From simulation with two different source spectra, 91-101 multiple events were generated in the same amount of time for temperature, T=40^oC. All detectors were placed in the same order as they were in the real setup, the lid that covers the source was also simulated. The number of multiple events,

Multiple Event results			
	Data (40^oC)	Simulation (Kluge & Weise)	Simulation (Geant4)
Number of detectors	30	32	32
Average active mass (g)	2475.84	2489.6	2489.6
RunLength (h)	177.6	177.6	177.6
Number of generated neutrons		43947690	43947690
Number of all bubbles	169710	163010	170935
Number of multiple events	98	91.26	100.76
Rate (c/s)	$(265.4\pm0.6)\times10^{-3}$	$(255.0\pm0.5)\times10^{-3}$	$(267.4\pm0.5)\times10^{-3}$
Efficiency (E_n^f)	$(3.86\pm0.01)\times10^{-3}$	$(3.71\pm0.01)\times10^{-3}$	$(3.99\pm0.01)\times10^{-3}$

Table 5.2: Results from measured data and simulation studies with 2 different spectra.

the efficiency of detectors and rates are corrected to the complete neutron processes physics list. In order to be sure about the number of multiple events from the data, another graph was produced that is called "Accidental multiple events" (Figure 5.11), to check if there are any single events that happened in that small range of time. An exponential equation 5.5 was used

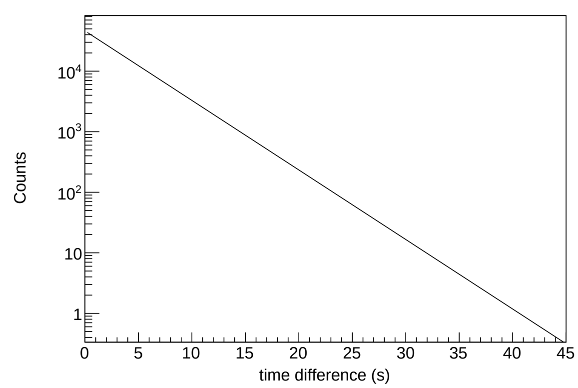

Figure 5.11: The time distribution between events.

$$N_{events} = N_{max} \exp(-R\Delta t) \tag{5.5}$$

where the R is the rate, total events divided by the total time in seconds. From the plot produced using equation 5.5, about 5-6 events in 100 microseconds were observed, which means that not all 98 events were multiple, but 5-6 events were accidental single events. Which results in 92.5 multiple events for 30 detectors or 98.7 events for 32 detectors. In total one expects to have between 91-101 events in 177.6 hours of calibration runs from simulation, which is in agreement with the empirical data of 98.7 multiple events.

The time distribution of multiple events, or in other words the time taken by a neutron to travel to another detector and cause an event after recoiling a fluorine in a certain detector is shown in the histogram in Figure 5.12.

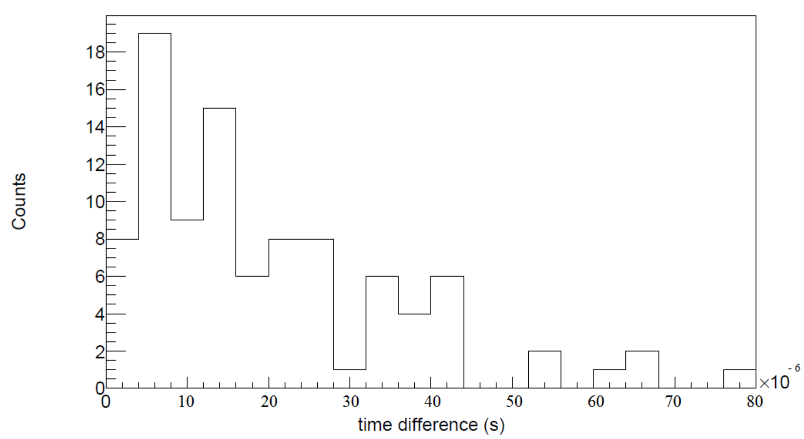

Figure 5.12: The time distribution between multiple events from data.

The multiple event study was repeated using the MC simulation, the time difference between multiple events from MC study is shown in Figure 5.13. There is a discrepancy between the two time distribution plots which comes from the speed of sound travelling inside the gel.

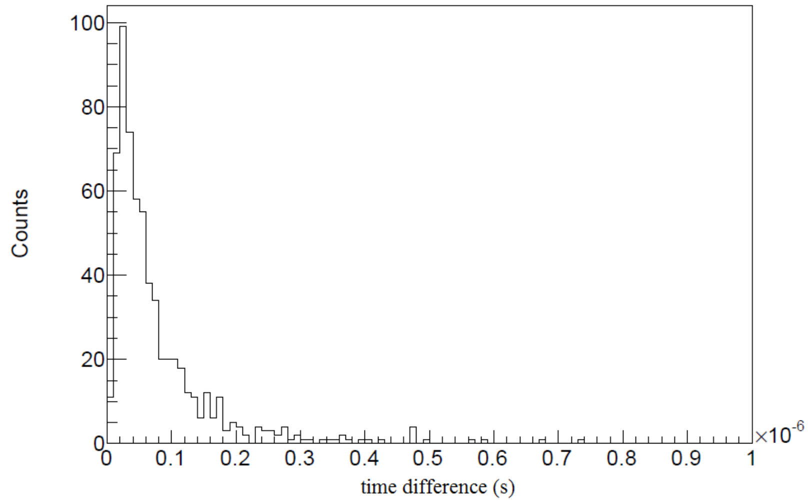

Figure 5.13: The time distribution between multiple events from MC simulation.

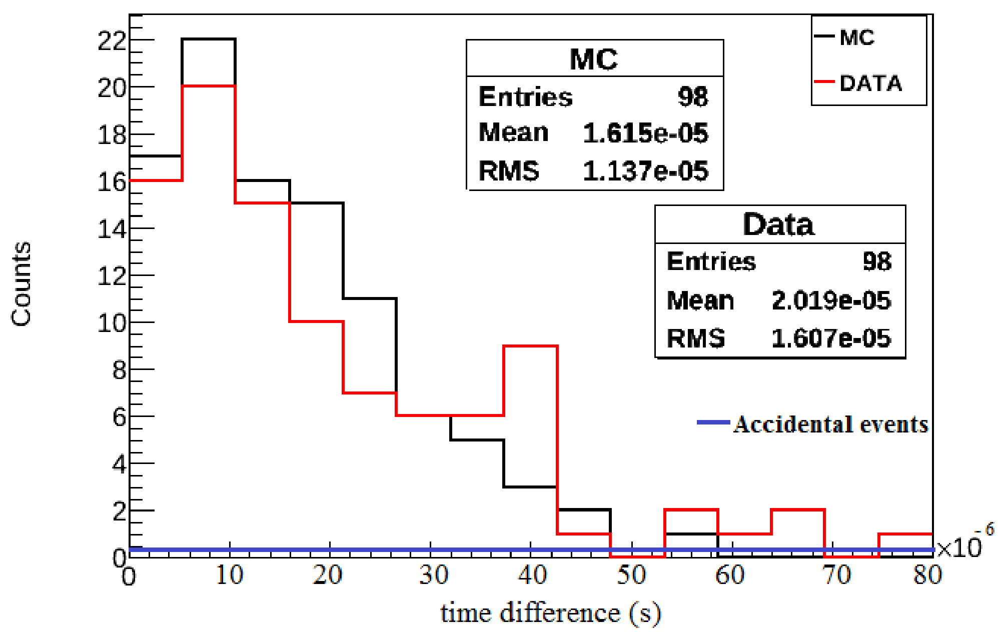

Figure 5.14: Comparison of the time distribution between multiple events between simulation and data.

The speed of sound in the gel is 1591 m/s according to PSTR-11-001 [28]. In comparison the speed of thermal and fast neutrons which have energies ranging from 1keV to 1MeV vary between 437 km/s to 14 000 km/s. Clearly, therefore, a neutron can create a multiple interaction before the sound from first neutron interaction is detected by the piezos. That is why Figures 5.12 and 5.13 show time difference plots differently. Another simulation was performed by taking the above mentioned time taken for the sound to travel inside the detector to the closest piezo into account. In this new simulation the location of each multiple event was recorded and the time difference between multiple events was calculated so that it includes the time of travel of a neutron from one detector to another and the sound propagation inside the gel to the piezos. Time difference plots of simulated and empirical data are compared and shown in Figure 5.14, where the empirical data agree with the simulation well. Events which happened in longer time frame in the same figure, which are located after 50×10^{-6} seconds are most likely accidental single events that occured within a very short time.

In conclusion, one can state that the results of simulation and empirical data are in very good agreement. The numbers of bubble events can easily be predicted using simulation results for future calibration runs, even the propagation and the time of neutrons to travel from one detector to another are well understood. The multiple events simulation works well and multiple events in PICASSO detectors in calibration data are expected to occur. The study has verified the simulation once more, one could also measure the efficiency (E_n^f) of detectors independently using the multiple events study. Knowledge about neutron rates and propagation of neutrons inside PICASSO was aquired. The efficiency of detectors from multiple events study, where the efficiency is the ratio of the total number of events to the total number of neutrons generated at the source, is between 3.71×10^{-3} and 3.99×10^{-3} and is in agreement with efficiency from measured data, which is 3.86±0.01 $\times 10^{-3}$.

5.E.2 Multiple interactions in WIMP Data

Using the same method, WIMP data (data taken without any particle source) was analysed for the temperatures where sufficient data existed. The runs were performed using a 30^oC, 35^oC, 40^oC and 45^oC temperature. Those bubbles with the time difference between two next events less than 0.1s and 0.0001s were determined. In order to verify the results, the number of accidental single events, which is labeled as "expected", were also calculated. All the results are shown in Table 5.3. To calculate the number of expected events an equation 5.5 was used, where there are two unknowns, N_{max} and Δt. By adjusting these two unknowns, and finding the integral, one is able to calculate the expected number of events with small uncertainity.

Another simulation of the PICASSO experiment was performed to see if neutrons from the host rock cause multiple events inside the detectors. Neutrons were simulated by only looking at the number of multiple events for temperature T=40^oC, with a run time equivalent of 69 years. 38,158 single events, with 20 multiple events were observed. This implies that no multiple events from neutrons coming from the host rock are expected in the data. The results of simulation and measured data cannot be directly compared, because the data includes neutrons, alphas, spallation from muons and noise, where the simulation only has neutrons from the rock. On the other hand, the number of events with time difference less than 0.1s and 0.0001s do agree with

Study on WIMP data to find multiple events				
	WIMP data			
Temperature (^oC)	30	35	40	45
RunLength (h)	926.5	781.5	2354	883.6
Number of bubbles	8805	6217	32905	31095
Number of events with tdiff (data)<0.1s	9±3	7±2.6	25±5	50±7.1
Number of single events with tdiff<0.1s (expected)	6±3	5±2	30±5	53±7
Number of events with tdiff<0.0001s (data)	0	0	1±1	1±1
Number of single events with tdiff<0.0001s (expected)	0.006	0.005	0.03	0.05

Table 5.3: Multiple interactions of neutrons in WIMP data.

the calculated number of accidental single events. In summary, no multiple events from neutrons, or muon induced neutrons were observed, in the current measured data set.

5.F Detector Stability

This section presents the change of efficiency of bubble detectors during the time of operation, using neutron calibration results from Monte Carlo simulation and data taken in 2009-2010 from the old utility setup. The main objective of this work was to study the detector response from the AmBe neutron source, check the efficiency of the detectors which are used for the experiment, and to find a solution for rate fluctuations in the measured data. A second objective was to study the propagation of neutrons inside PICASSO and verify the source positioning.

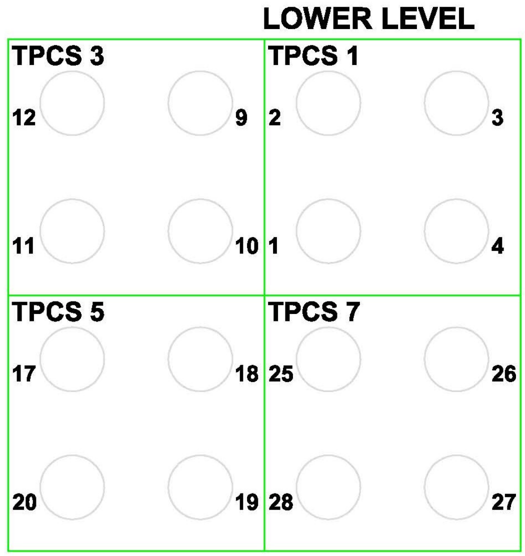

Figure 5.15: Location of detectors in the lower level of the PICASSO setup.

A simulation with an AmBe neutron source at the center of each TPCS is performed. The detectors of TPCS #1 are moved 2.25 cm from their original position to simulate the effect of a small detector position discrepancy on the number of bubbles in the detectors. It is obvious that detectors of TPCS #1 will be affected a lot when the source is in TPCS #1 and detectors are moved. The same effect, but smaller, is seen for detectors in TPCS #1 when the source was placed in TPCS #3 and TPCS #7, but no effect was observed when the source was in TPCS #5. A graph showing the effect of position discrepancy on a detector is shown in Figure 5.16.

Using the slope of the above plot and similar plots for other detectors one can create equation 5.6, which can be used to determine the error in the position of the detectors.

$$Rate = N_{source} E_g E_0 (1 + m_x * X + m_y * Y)/m_F \tag{5.6}$$

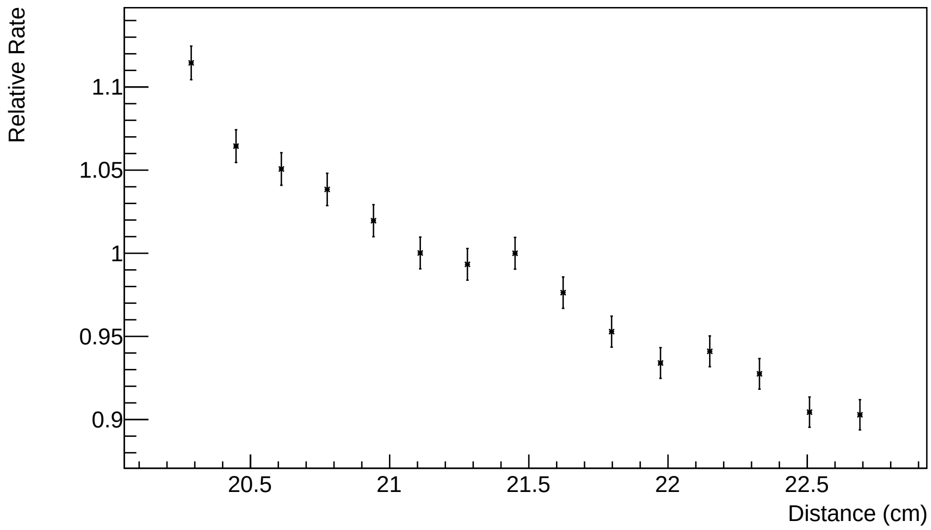

Figure 5.16: Relative change in number of counts in detector #1 when it is moved around its original position in x direction. The source is in TPCS #1.

where m_x, m_y are the slopes of a detector moving in x and in y directions respectively, and X and Y are the position of a detector away from its' original position, m_F is the mass of fluorine in the detector, N_{source} is the number of neutrons the source emits in 1 hour, E_g geometrical effect of neutrons to propagate from one TPCS to another one, E_0 is the neutron detection efficiency. Using the available empirical data and assuming that the detectors are located in their nominal positions, the E_0 of detectors were calculated. Getting geometrical efficiency, E_g, for all detectors from simulation and by comparing them with data, it was observed that the geometrical efficiencies of the detectors are almost the same for simulation and for data. For example, the geometrical efficiency of detector #1 from the source located in TPCS #3 is 0.441, which is the same for the source in TPCS #7 and also agrees with the data. It is impossible to study the detector stability for all detectors, be-

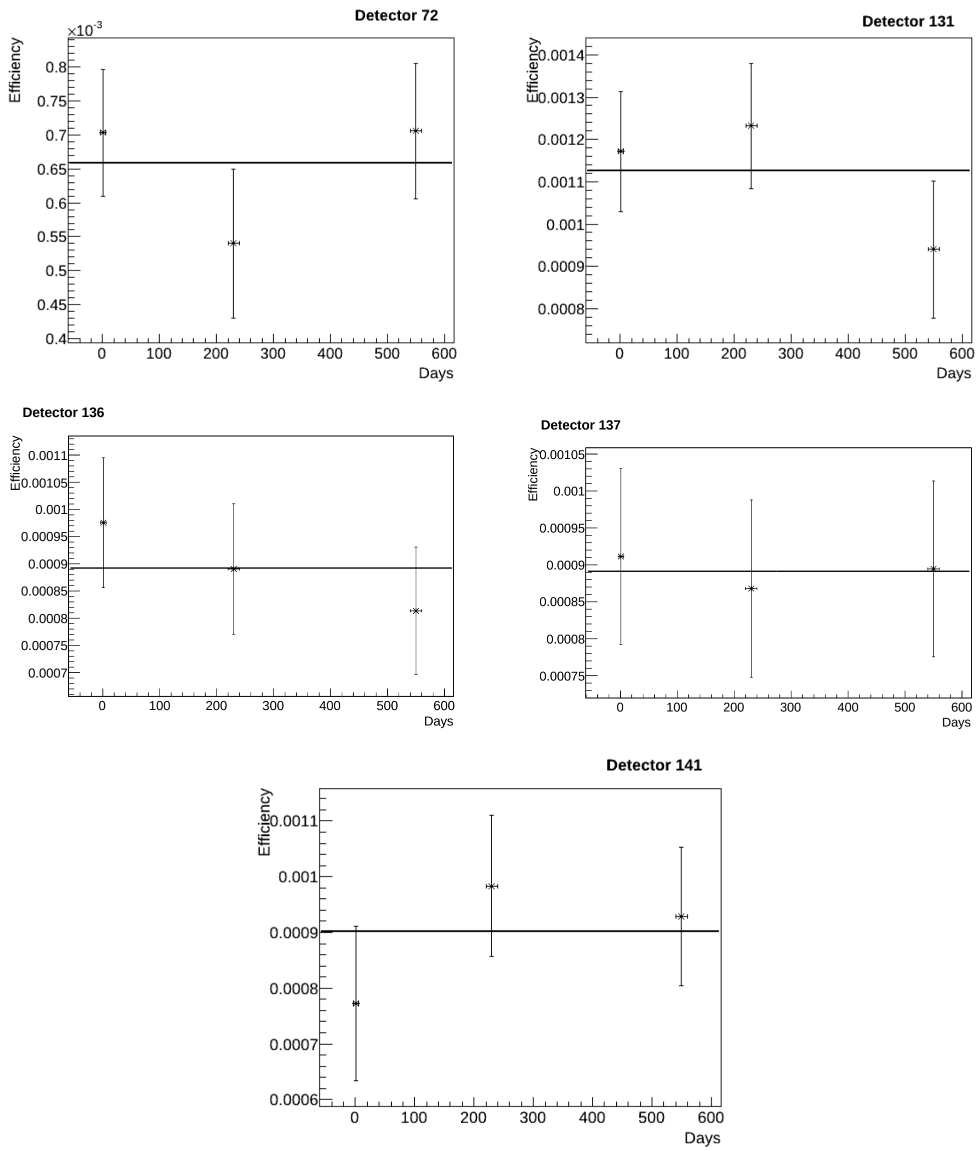

Figure 5.17: Efficiency as a function of time of "good" detectors between February 2009 and August 2010.

cause there are some detectors with less active mass, there are some with large background and some with electronics problems. By inserting all known terms of certain detectors into equation 5.6 and using the Minuit Root minimization package it was easy to find the efficiencies of these detectors throughout the operation for runs calibrated at $40^{o}C$. In the old utility setup there are 3 different time ranges of calibrations at 40^oC. The change in efficiency as a function of time for some calibrated and good detectors are shown in Figure 5.17. The uncertainity bars in the plots include the pressure change uncertainity and the source positioning and orientation uncertainities.

By analyzing the data and looking at the plots, one can clearly see that the efficiency of detectors does not change over time and it is stable for all 5 detectors.

5.G Environment influence

5.G.1 Effect of varying active mass to fluorine recoils

PICASSO uses ^{19}F as an active material, in each detector volume there is on average about 80g of ^{19}F. All currently used detectors differ by the mass and the number of C_4F_{10} droplets that are immersed inside. To calculate the rate and the efficiency for every single detector, the detectors in the simulation should contain exactly the same amount of active material as it is in reality. However, the Geant4 code of PICASSO has the same amount of droplets in each detector, which is 77.6 g per 4.5 L of cesium chloride gel or polymerized gel with glycerine and polyethylene glycol as the main ingredients. In order to determine if the efficiency is proportional to the active mass (m_{ac}), another study was done, where in simulation the amount of active mass in the detectors was changed repeatedly. Figure 5.18 shows that the number of events is proportional to the active mass. The fit equation will help to find the expected number of events for all detectors knowing just the active mass. The equation of this fit from the graph is $N = (50198.8 \pm 302.916)m_{ac} - (87.5974 \pm 273.853)$.

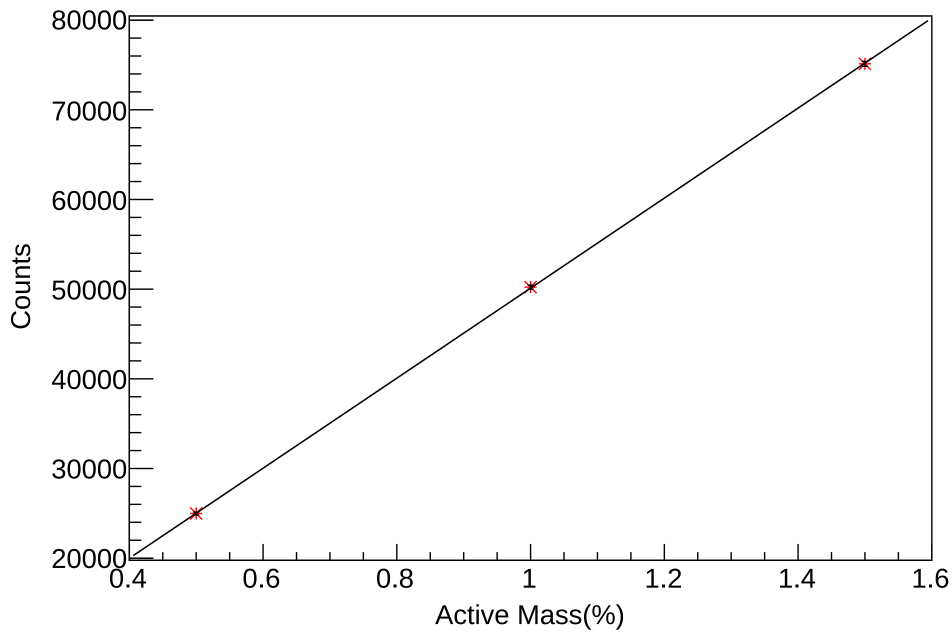

Figure 5.18: Counts as a function of active mass from the MC simulation.

5.G.2 The rate discrepancy of saltless and salty detectors

There are two types of detectors that PICASSO uses: a detector with salty gel (CsCl) and a detector with saltless gel (polymerized gel with glycerine and polyethylene glycol).

- The density of saltless gel is $1.057 g/cm^3$. Saltless gel is made of hydrogen, carbon, oxygen, nitrogen and fluorine.

- The density of salty gel is $1.57 g/cm^3$. Salty gel or cesium chloride gel is made of hydrogen, carbon, oxygen, nitrogen, chlorine and cesium.

Saltless gel contains about 7.5% of hydrogen, where salty gel contains 5.5% of hydrogen, which leads to discrepancies in count rates of salty and saltless detectors, since the neutron cross-section of hydrogen is large. Even though both types of detectors have the same amount of C_4F_{10} the number of recoils in salty and saltless detectors in neutron calibrations will be different. From the simulations done using only salty and only saltless detectors the following numbers were generated: for salty detector 57092 counts and for saltless 50471 counts out of 12.4×10^6 events generated, which is an 11.6% discrepancy for all 32 detectors combined.

When a neutron enters a detector it is possible for it to interact with all particles inside the gel, the neutron interaction probability for all particles in the salty gel is shown in Table 5.4. The neutron interaction probability with particles inside the saltless gel is shown in Table 5.5.

Partice	Mass %	Neutron Cross-Section (b)	Recoiled secondary particles (%)
Hydrogen (H)	5.538	82.02	74
Carbon (C)	1.675	5.559	1.16
Oxygen (O)	42.248	4.232	18.7
Nitrogen (N)	0.528	11.53	0.23
Chlorine (Cl)	10.321	21.8	1.9
Cesium (Cs)	38.69	0.782	3.5
Fluorine (F)	1	4.018	0.33

Table 5.4: The percentage of recoiled particles in salty detectors.

Particle	Mass %	Neutron Cross-Section (b)	Recoiled secondary particles (%)
Hydrogen (H)	8	82.02	75.6
Carbon (C)	16	5.559	4.78
Oxygen (O)	73.9	4.232	19.05
Nitrogen (N)	1.	11.53	0.3
Fluorine (F)	1.1	4.018	0.28

Table 5.5: The percentage of recoiled particles in saltless detectors.

In summary, the saltless detectors are found to be less likely to observe a neutron event than salty detectors.

5.G.3 Effect of the water and self shielding on the rate in detectors

When the neutron AmBe source is put in the center of a TPCS and a neutron emitted from the source travels through the PICASSO experiment, it travels through steel plates, acrylic containers, aluminum boxes and it definitely travels through the gel inside the detectors. Most neutrons loose the majority of their energy in a single interaction with the surrounding material. However some neutrons are so energetic that they can interact, scatter, interact again and scatter again. Using this simulation results, 4 detectors with an equal

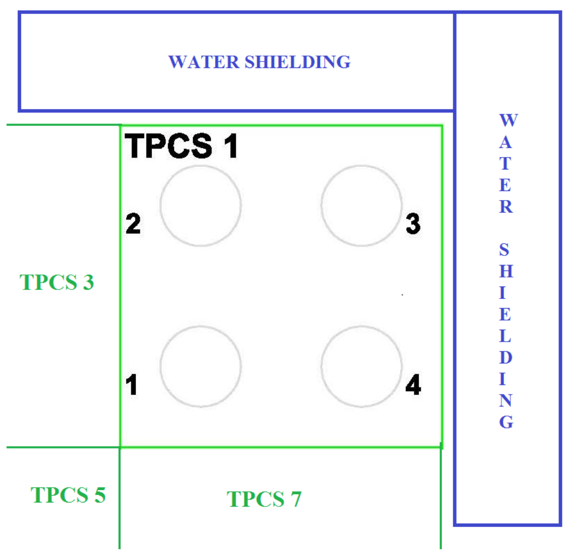

Figure 5.19: Location of TPCS1 in experiment, right and upper side of TPCS 1 is surrounded by water shielding, and on the left and lower sides there are other TPCS's with detectors in it.

amount of gel and an equal amount of active mass found to have have different number of recoils, when the surrounding geometry was changed. When there is more shielding-material surrounding the detectors the rate in the detectors increases, because there will be a chance for the neutrons to come back after interacting with other materials. In Figure 5.19 the orientation of TPCS 1 and the position of each detector in the experiment is illustrated. Four simulations using all neutron physics processes, neutron elastic, inelastic interactions and neutron capture were done. The temperature is kept at 55 ^{o}C and the source position is in the center of TPCS 1, unchanged for all the studies. In one simulation there is only detector 1 in TPCS 1, all other detectors and the water shielding are removed. In the second there are only 4 detectors in TPCS 1 with no shielding. In the third and fourth simulations all the detectors are simulated, while in third there is no water shielding and in fourth there is shielding. Each simulation used 23.7 million neutrons emitted from the source which corresponds to 100 hours of source running, at $55^{o}C$. The results are shown in Table 5.6.

	det 1	det 2	det 3	det 4
1 detector only	16431			
4 detectors only	17755	18001	17718	17976
32 detectors only	18270	18037	18193	18229
32 detectors and shielding	18594	18501	18755	18546

Table 5.6: Number of counts in each detector for different code geometry.

There is an 11.6±0.2% difference between the set-up when detector 1 is placed alone and the realistic setup with all 32 detectors and shielding. When there is shielding detector 3, which is located in the corner next to the water shielding has more recoils than detector 1 by 1.1±0.1 %. When there is no shielding the number of counts in detector 1 is similar to the number of counts in detector 3. Detectors that are located next to water shielding, or next to other materials, have a larger number of recoils than solitary detectors, which leads to the conclusion that the water shielding affects the rates in PICASSO bubble detectors. It means that neutrons interacting inside the water can be reflected and cause an event in detectors located next to shielding.

5.G.4 Systematic uncertainities of the neutron source

Source position

To test the influence of the AmBe source location, a new simulation was performed using Geant4 by changing the position of the source. Four different simulations are done at 40^oC, moving the source by 2cm away from the center of TPCS 1 in different directions. The position of the source inside the TPCS and the number of counts in detectors inside that TPCS is shown in Table 5.7.

Source Position (x(cm), y(cm), z(cm))	det1	det2	det3	det4
0, 0, 0	0	0	0	0
-2, 0, 0	+11.1%	+10.6%	-9.7%	-9.7%
2, 0, 0	-9.5%	-10.1%	+10.9%	+11.0%
0, 2, 0	-9.7%	+10.7%	+10.8%	-9.5%

Table 5.7: The effect of source positioning on the number of recoils in detectors.

Table 5.7 shows a ~10% discrepancy in each direction for any detector for a 2cm misplacement of the source. This means that a small source positioning uncertainity can lead to a large deviation in detector rates.

AmBe source can

For neutron calibrations PICASSO uses an AmBe neutron source, where the source is enclosed in a can. The can is made of substance called Delrin (Polyoxymethylene), which has the molecular formula of $(CH_2O)_n$ where n≈9 and its density is $1.45 g/cm^3$. Since the can is made of a hydrogen-rich material, it is expected to be blocking neutrons. As a result it is expected to see less events in detectors when there is a Delrin can. According to this simulation, about 4 neutrons out of 10 interact with Delrin before leaving the can, obviously neutrons loose energy and become slower. According to the simulation, about 3% of the neutrons cannot pass through the can. In Figure 5.20 the spectrum change of the neutron source with the Delrin can is illustrated . When there is

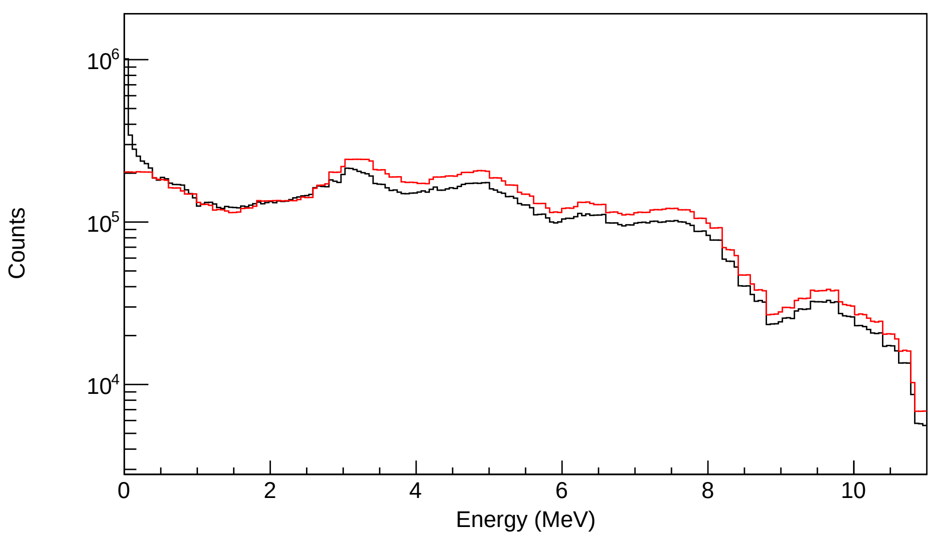

Figure 5.20: Energy spectrums of neutron source with(black line) and without(red line) Delrin are compared.

a Delrin can, the number of fluorine recoils decreased and the total rate goes down by 4% compared to the un-covered neutron source. The mean energies of neutrons that interact with fluorine are $1.23 \pm 0.02 MeV$ when there is no can and $1.19 \pm 0.02 MeV$ when Delrin surrounds the source. To sum up, the Delrin can softens the neutron energy and decreases the rate in the detectors by 4%.

Source orientation

The source can is a tube shaped material made of Delrin. One edge of the can is thicker than the other edge, which has a large effect on neutron rates in detectors if the source orientation is changed. One expects to see more interactions in the direction of the thicker side of the can than the other side, neutron particles coming from the center of the source interact more on the thick side and loose more energy. In this section, the word "cap" was used to refer to thicker side of the source can. A simulation was done to test the effect of the source can to detector rates when placed in different orientations. The temperature is 55^oC and the total number of events generated for each orientation is 2.4 million events. From Table 5.8 one can see the number of neutron interactions in detectors for each source orientation. The position of detectors inside the setup is shown in Figure 5.15.

Det.	No Cover	Cap towards right	Cap towards TPCS 3 (left)	Cap towards TPCS 2 (up)	Cap towards detector 2	Cap towards detector 1
1	2127	2041	2015	2165	2165	1576
2	2173	2005	2014	2218	1675	2252
3	2183	2054	2008	2160	2186	2252
4	2154	1998	1973	2225	2182	2186

Table 5.8: Number of neutron recoils in detectors for different source orientations.

As it can be seen from the table, if the cap is pointed to any detector there is about 25% difference in the number of recoils for detectors inside the same TPCS and about 15-30% difference for detectors in other TPCSs. In order to calibrate neutrons one should always put the source in one direction. The source cap can be placed in such a way that it points the ceiling for all further

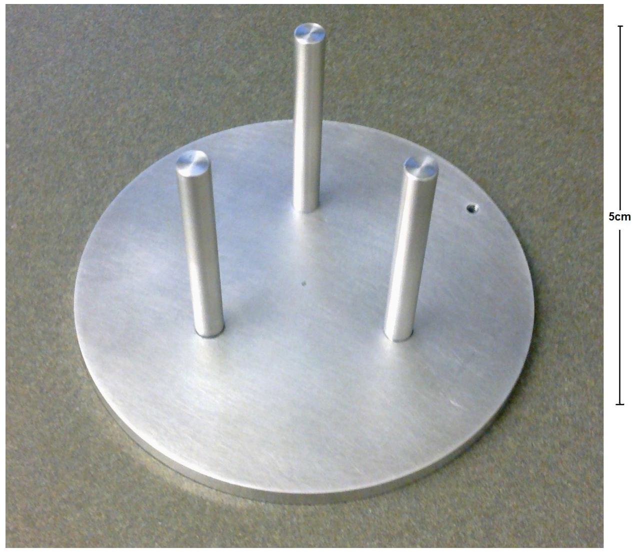

Figure 5.21: New designed source holder to put an AmBe source inside.

calibrations in the new installation. A source holder, which was designed and built at the University of Alberta, which is shown in Figure 5.21, will be used for further calibrations. It is made of aluminum, because of its low neutron cross-section.

5.H Localisation of bubbles inside the detectors

A new project called "localisation of events" is in progress at the time of writing. This project is designed to study each bubble signal received by the piezos and to localize them inside the detector to get more information about the nature of the signal. Theoretically a detector with no background should always stay calm without any bubble burst, unless a WIMP causes them. In reality, there are background sources such as alpha particles, background neutrons and other enviromental processes which can trigger the detectors.

Run number	Run length (h)	Temperature (^oC)	Position of the source (TPCS #)	Detectors studied
0.5601.4	4	45	2	131, 137, 144, 151
0.5615.4	1	45	7	153, 154, 155, 156
0.5655.4	1	45	1	141, 145, 147, 148

Table 5.9: Detectors and data used in localisation study.

In some parts of the gel inside the detectors there might be lots of triggers which are called "hot spots". To discriminate these events from each other and to be able to say if the gel is homogeneous, each event inside a detector is localised. For example, if there are events next to the acrylic walls, they might be coming from surface alpha particles and they can be discriminated. Or if a certain part of the gel has more events than other parts of the gel, events which happened in that part of the volume can be excluded. For this study, the empirical data from the new installation was used. Therefore the code for the new installation was used to simulate neutron calibration runs.

Using two different algorithms of localisation the PICASSO collaboration is now able to study the positions of each event [30], [8]. To examine the localisation algorithms the PICASSO experiment was simulated once more.

First of all, 3 different calibration runs which meet quality requirements were chosen. In each run, the neutron source is in a different TPCS, so that it was possible to study all 12 detectors. Chosen runs, position of the source in each run and studied detectors in each run are shown in Table 5.9.

From a simulation where the source was in TPCS 7, the location of events graphs were generated which is shown in Figure 5.22. The plots show clearly that the source was in the middle of these 4 detectors.

For empirical data, if the localisation algorithms are valid, one expects

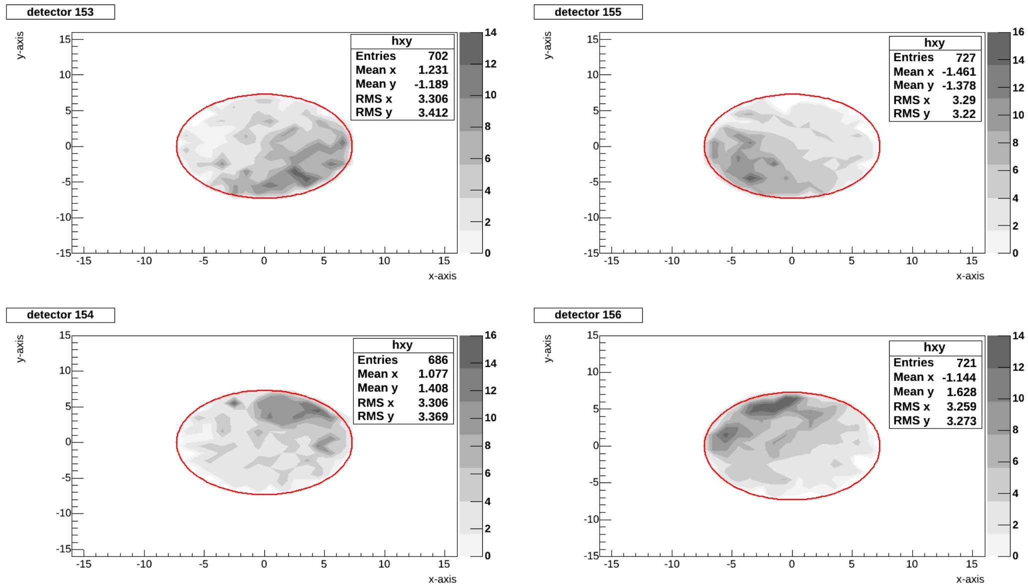

Figure 5.22: The localisation of events inside detectors of TPCS 7 (Monte Carlo).

the same neutron distribution. Taking the speed of sound to be 1704 m/s the localisation of events were constructed for data points, which is shown in Figure 5.23, where the neutron distribution is almost the same as in the simulation.

There are discrepancies between the data and MC in mean x and mean y values in the plots. The discrepancy can be explained by source positioning, detector orientation and the finite reconstruction resolution. The exact localisation resolution has not been fully studied yet. When detectors are moved or replaced, they get rotated and moved, which causes some of these discrepancies. For further calibration runs PICASSO always has to check the orientation of detectors and piezo locations. There is also some uncertainity in the speed of the sound which was used to locate the events, this can cause events to be shifted from their expected position.

In general the distribution of neutrons inside the detectors are similar for

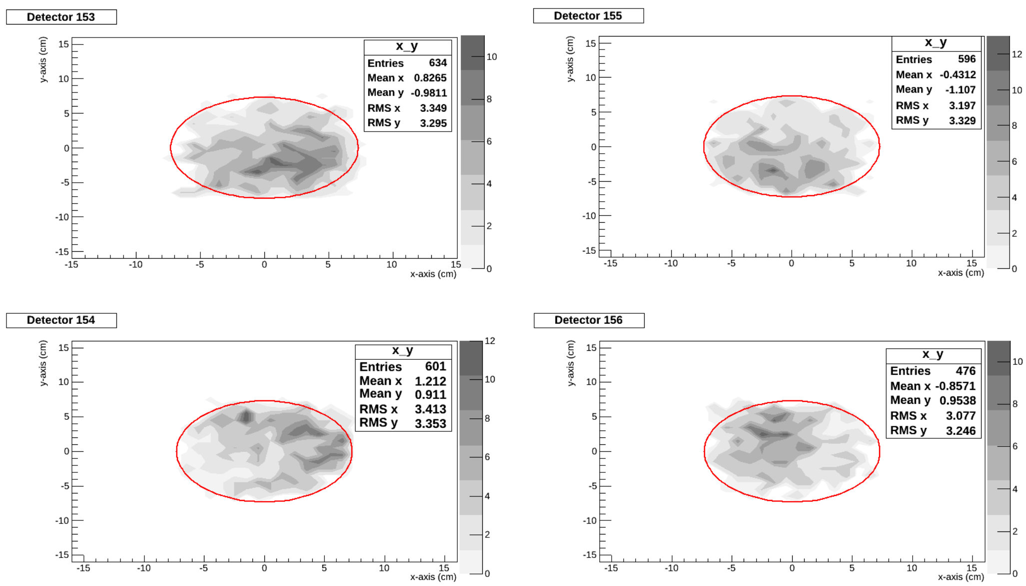

Figure 5.23: The localisation of events inside detectors of TPCS 7 (data).

simulation and for experiment. Which tells that localisation algorithms of PICASSO work, and reconstruction of events using these methods can now be performed. This also verifies the simulation.

5.I pVar vs mean energy as a function of distance

A nuclear interaction of a neutron with ^{19}F inside a detector creates an acoustic signal which is then received by piezos. Frequency and amplitude of such acoustic signals are expected to be identical to each other, however the gel inside the detector can affect the signal information. This study explores whether a signal created as a result of a neutron ^{19}F interaction depends on the energy of the neutron. According to simulation results the average neutron energy changes as a function of distance. In Figure 5.24, a graph with the mean energy of neutrons that interacted with ^{19}F as a function of distance from the source for all 32 detectors is shown (from the MC simulation).

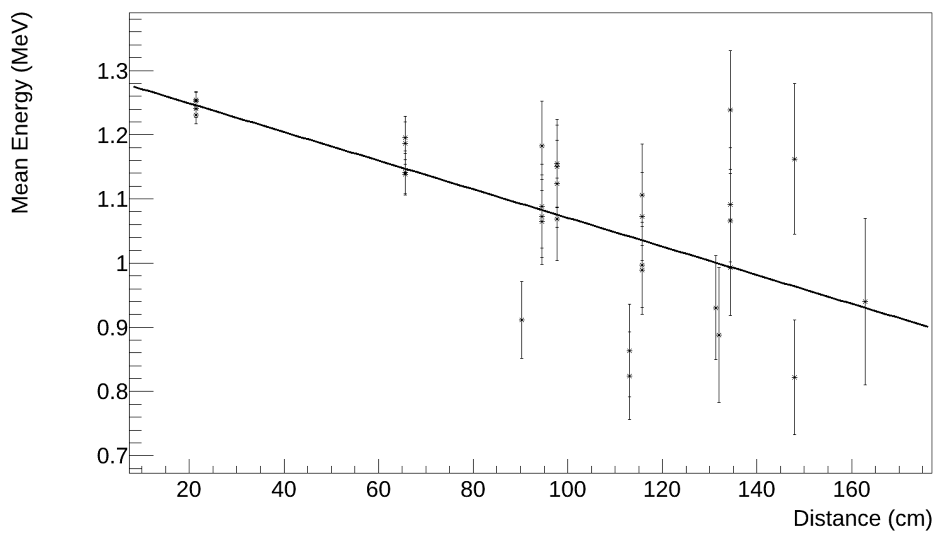

Figure 5.24: Average energy of neutrons that created an event as a function of distance from the source.

Pvar, which measures the acoustic power of an event is shown as a function of distance in Figure 5.25. For all three studied detectors it is clearly visible that pvar is contstant as a function of distance, which means pvar does not depend on neutron energy.

As a result, it was found that the pvar of a signal does not depend on the energy of neutrons.

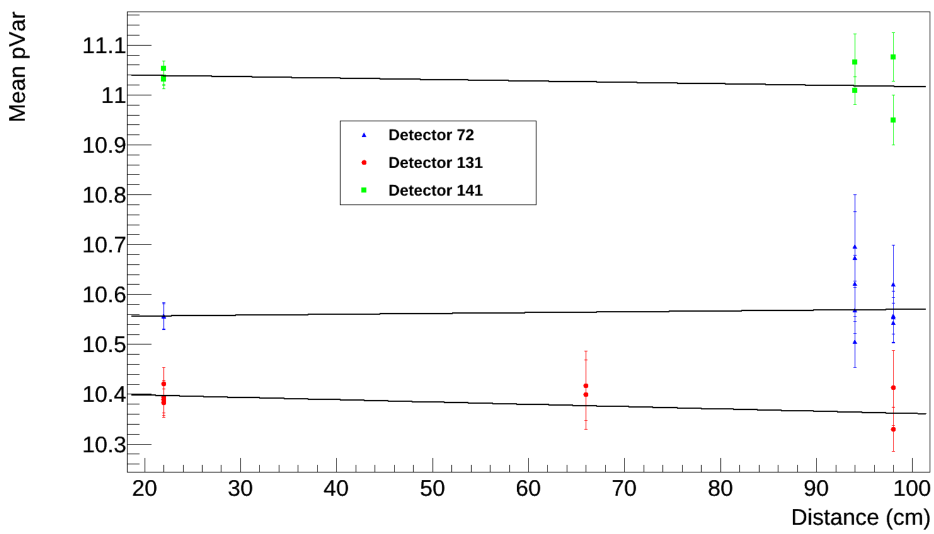

Figure 5.25: Average pvar as a function of distance for some detectors.

Chapter 6

Conclusions

It was shown that the contribution of neutrons from the rock is lower than 1-2 neutrons/day for the utility room setup. This is well below the background count rate recorded in the utility room setup. This study only uses elastic neutron interactions and therefore only provides an upper limit. For the new installation the number of neutrons coming from the rock is less than 0.1 neutrons/day. The shielding efficiency for the new installation is significantly improved over the shielding of the old setup. Moreover the agreement of simulation results with the results from a simulation of Kamaha's Monte Carlo studies verifies this simulation of PICASSO. Neutrons from the surrounding rock are not a relevant background source.

The number of events for different AmBe neutron source spectra differ by 10%. Neutron rates in each detector for different physics lists (types of simulated neutron interactions) vary between 2.5% and 5%. Once in 0.19 kg day exposure multiple neutron interactions are expected to occur using the SNO 68.71 neutron/s source. No multiple events were detected with WIMP runs. In the past the collaboration simply assumed that the detectors would be stable over time. The results showed that the efficiency of detectors studied stays constant through 1.5 years of operation, which validates the assumption. The stability study suffered significantly from source positioning uncertainities. To keep the source from moving and rotating, and to improve source position and orientation uncertainity, a new source holder was designed. For calibration runs taken after July 2012 this source holder will be used.

Salty detectors are more sensitive to neutrons than saltless detectors since they contain less hydrogen. In addition, materials and shielding surrounding the detector change the number of events from an internal neutron source by up to 11%. Moreover, simulation shows that the localisation algorithms of the PICASSO collaboration work. Neutron distributions from simulation are the same as from the experiment, which again verifies the simulation. Finally, the measured data show that the power amplitude of a signal does not depend on the energy of a neutron.

This study also extracted an efficiency value for the complete PICASSO detector system from multiple neutron interactions. This extraction is independent from the assumed neutron spectrum of the neutron source and falls between the efficiencies determined by a full neutron simulation of the PICASSO detector and its shielding. The average efficiency of all detectors combined of the old setup was found to be $(3.86\pm0.01)\times10^{-3}$ from experimental multiple events studies, whereas from the Monte Carlo studies the efficiency of neutron-fluorine recoils was found to be $(3.71\pm0.01)\times10^{-3}$ using the Kluge & Weise spectrum and $(3.99\pm0.01)\times10^{-3}$ using the Geant4 example spectrum.

Ultimately the availability of a well vetted neutron simulation for the PICASSO experiment will allow the collaboration to improve the understanding of external and internal neutron backgrounds. This will allow to understand the floor of the achievable backgrounds in the current PICASSO setup. It will also improve the sensitivity to dark matter interactions, because it will allow PICASSO to improve the understanding of neutron-flourine interactions at all energies and thereby reduce the uncertainty that is associated with the probability of creating a bubble that changes with threshold and therefore with temperature.

Bibliography

[1] S. Agostinelli et al., "GEANT4 - a simulation toolkit", *Nuclear Instruments and Methods in Physics Research A, 506, p. 250-303*, 2003.

[2] J. Allison et al., "Geant4 Developments and Applications", *IEEE Transactions on Nuclear Science, Vol. 53, No. 1*, February 2006.

[3] E. Aprile et al., "First Dark Matter Results from the XENON100 Experiment", *Phys. Rev. Lett. 105.131302*, March 2011.

[4] S. Archambault et al. , "Constraints on Low-Mass WIMP Interactions on 19F from PICASSO", *Physics Letters B, Volume 711, Issue 2, p. 153-161*, March 2012.

[5] S. Archambault et al., "New Insights into Particle Detection with Superheated Liquids", *New Journal of Physics, Volume 13, Issue 4, 043006 (25pp)* , April 2011.

[6] S. Archambault et al., "Dark Matter Spin-Dependent Limits for WIMP Interactions on ^{19}F by PICASSO", *Physics Letters B, Volume 682, Issue 2, Pages 185-192*, November 2009.

[7] F. Aubin et al.,"Discrimination of nuclear recoils from alpha particles with superheated liquids", *New Journal of Physics 10 103017 (11pp)*, October 2008.

[8] F. Aubin, "Caracterisation spatiale des evenements dans les detecteurs PICASSO", *M.Sc.Thesis*, Universite de Montreal, April 2007.

[9] M. Barnabe-Heider et al., "Response of Superheated Droplet Detectors of the PICASSO Dark Matter Search Experiment", *Nucl. Instrum. Meth. A555, pp. 184-204*, 2007.

[10] L. Bergstrom, "Dark Matter Candidates", *New Journal of Physics 11:105006*, 2009.

[11] K. J. Clark,"A New and Improved Spin-Dependent Dark Matter Exclusion Limit Using the PICASSO Experiment", *Ph.D. Thesis*, Queens University, July 2008.

[12] W.F. Davidson et al, Background Measurements in the Creighton Mine, *ANNEX 10*, copy available at `https://picassoweb.lps.umontreal.ca/elog/Weekly+Meetings/111219_121417/DOC.PDF`, 2011 .

[13] J. Ellis and K. A. Olive, "Supersymmetric Dark Matter Candidates", from book "Particle Dark Matter: Observations, Models and Searches", ISBN 9780521763684, *arXiv:1001.3651v1 [astro-ph.CO]*, January 2010.

[14] P. Fisher, "Dark Matter", available at `http://www.learner.org/courses/physics/unit/text.html?unit=10&secNum=2`, January 2012.

[15] J. L. Feng, "Dark Matter Candidates from Particle Physics and Methods of Detection" *Annu. Rev. Astron. Astrophys. 48, pp. 495545*, May 2010.

[16] G. Jungman et al., "Supersymmetric Dark Matter", *Physics Reports 267, pp. 195-373*, 1996.

[17] A. C. Kamaha, "Study of the Neutron Background", PICASSO collaboration internal document available only for PICASSO members at `https://picassoweb.lps.umontreal.ca/elog/Weekly+Meetings/268`, Queens University, December 2011.

[18] H. Kluge, K. Weise, "The Neutron energy spectrum of a $^{241}Am{-}Be(\alpha, n)$ source and resulting mean fluence to dose equivalent conversion factors.", *Radiation Protection Dosimetry Vol. 2 No. 2 p.85-93 Nuclear Technology Publishing*, February, 1982.

[19] L. Lebreton, A. Zimbal, D Thomas, "Experimental Comparison of $^{241}Am - Be$ Neutron Fluence Energy Distributions", *Radiation Protection Dosimetry, Vol. 126, No. 1-4, pp. 3-7*, May 2007.

[20] C. Levy, "Gamma Calibration Using A New Test Apparatus At Queens University And Optimization Analyses For The PICASSO Experiment", *M.Sc.Thesis*, Queens University, September 2009.

[21] Y.F. Li, Z. Z. Xing, "Neutrinos as a hot or warm dark matter", Proc. of the conference "Matter to the Deepest", *arXiv:1110.2293v1 [hep-ph]*, October 2011.

[22] R. Massey, Thomas Kitching, Johan Richard, "The dark matter of gravitational lensing", *Rep. Proj. Phys. 73.086901*, 2010.

[23] D.M. Mei and A. Hime, "Muon-induced background study for underground laboratories", *Phys. Rev. D 73, 053004*, 2006.

[24] A. H. G. Peter, "Dark Matter: A Brief Review", Proc. for the Frank N. Bash Symposium (2011), available at *arXiv:1201.3942 [astro-ph.CO]*, 2012.

[25] J. R. Primack, "Hot Dark Matter", from book "Encyclopedia of Astronomy & Astrophysics", ISBN: 0333750888, available at `http://www.astro.caltech.edu/~george/ay21/eaa/eaa-hdm.pdf`, 2006.

[26] W. Rau, "Dark Matter Search Experiments", Proc. of "Physics of Elementary Particles and Atomic Nuclei", *arXiv:1103.5267v1 [astro-ph.CO]*, March 2011.

[27] P. Rinard, "Neutron Interactions with Matter", Passive Nondestructive Assay of Nuclear Materials, (Ed. by Doug Reilly et al.), *Nuclear Regulatory Commission, NUREGKR-5550. pp. 357-377*, 1991.

[28] J. S. Roberge, "Speed of Sound in the Saltless gel", *Technical Report, PSTR-11-001*, Laurentian University, April 2011.

[29] R. W. Schnee, "Introduction to Dark Matter Experiments", Proc. of the 2009 Theoretical Advanced Study Institute in Elementary Particle Physics, *arXiv:1101.5205 [astro-ph.CO]*, 2010.

[30] C. Storey, "The Development of an Event Localization Algorithm for the PICASSO Dark Matter Experiment", *M.Sc.Thesis*, Queens University, May 2007.

[31] D.R. Tovey et al., "A new model-independent method for extracting spin-dependent cross section limits from dark matter searches", *Physics Letters B 488, pp. 1726*, August 2000.

[32] H. R. Vega-Carrillo et al, "Neutron and gamma-ray spectra of $^{239}PuBe$ and $^{241}AmBe$", *Applied Radiation and Isotopes 57, Issue 2, pp. 167-170*, August 2002.

[33] B. Winstein, "The Cosmic Microwave. Background Radiation", SLAC Summer Institute Lecture, University of Chicago (Supported by the NSF), 2004.

[34] V. Zacek, "Dark Matter", Proc. of Lake Louise Winter Institute, *arXiv:0707.0472 [astro-ph]*, March 2007.

[35] "Cosmic Microwave Background Radiation" , available at http://en.wikipedia.org/wiki/Cosmic_microwave_background_radiation, 2012.

[36] "COUPP Dark Matter search experiment webpage", available at http://www-coupp.fnal.gov/, January 2012.

[37] "Cryogenic Dark Matter Search experiment homepage", available at http://cdms.berkeley.edu/, January 2012.

[38] "DEAP/CLEAN collaboration webpage", available at http://deapclean.org/, January 2012.

[39] Geant4 Simulation Toolkit by CERN, version 9.5 2nd release, available at http://geant4.cern.ch, downloaded on December 2011.

[40] The double Quasars image, available at http://www.astr.ua.edu/keel/agn/q0957.html, April 2012.

[41] PICASSO experiment public webpage, available at http://www.picassoexperiment.ca, 2012.

[42] Image of Vera Rubin's plot, available at http://www.theeternaluniverse.com/2010/06/great-history-of-evidence-for-dark.html, 2012.

[43] "The XENON Dark Matter Project webpage", available at http://xenon.astro.columbia.edu/, January 2012.